Please note that the reviewers' comments are in black and responses are in blue.

Editor

Comments to the Author:

Dear Dr. Biswas and co-authors,

Thank you for your clear responses to the referee comments on your Discussion manuscript and your willingness to consider their suggestions. I invite you to submit a revised manuscript in the spirit of your responses. Because the nature of the referee comments and your proposed manuscript changes are fairly technical, any revised manuscript will go through an additional round of peer-review (this additional round will not be open to the public, though eventually the reviews and responses become part of the public record). This requires that I indicate a decision of "major revisions" on this manuscript.

Sincerely,

Alberto Reyes (handling editor)

Non-public comments to the Author:

Just a few additional comments based on the reviews and my own reading of the manuscript:

1. I suggest rephrasing part of the paragraph beginning 4/30-31 of the original manuscript. Climate is a much longer term phenomenon than daily/season changes in conditions. And on longer timescales, climate does not follow Milankovitch forcing in a linear way but rather is paced by it. I realize that this section represents a theoretical exercise, but the way the section starts it would be easy for readers to get the wrong impression.

We have changed the sentence to "*Earth's climate varies in cyclical way, at multiple time scales from years to decades, centuries, and millennia, influenced by periodic variations in the Earth's orbit, known as Milankovitch cycles, at 25.77, 41 and 100 kyr*". See page 4, line 28-29 in the revised manuscript.

2. The first and second substantive comments from Rev 2 involve some potential misunderstanding of assumptions made in your study. I encourage you to provide additional clarity on these points in your revision.

Please see the replies to those comments the action taken in the manuscript.

Anonymous Referee #1

General comments:

The authors are investigating an interesting question–whether luminescence signals from K-feldspars in bedrock might archive changes in recent temperatures at Earth's surface. More specifically, they ask whether we can resolve recent changes in temperature periodicity. This question is important and worth pursuing.

I commend the authors for the layout of this study. Their approach involving sensitivity analyses, calibration to sample specific kinetics and attention to climatic complexity have resulted in an interesting manuscript with potential for significant scientific impact.

We appreciate the reviewer for discerning the potential of this work.

However, the present work needs significant clarification and expansion to yield a robust estimate of past temperatures. Specifically, the authors must determine how changes in amplitude, period, and mean temperature influence luminescence signal growth and depletion in a holistic way. Currently, the treatment is partial. Once this is done, the authors should give a more direct comparison of actual and predicted temperature histories in order for the reader to better examine the predictive success of the model.

Please see the replies below.

These points and others are detailed below.

1/22: "Earth's climate fluctuates in a cyclic way" While there are many internal cycles to climate systems, this characterisation might be too simplistic, especially at the timescales involved here (~10^1 - 10^2 kyr), where abrupt periods of change are common. Temperature changes during the Holocene, for example, can hardly be approximated as cyclic.

We have changed the sentence to… "*Earth's climate fluctuates in a cyclic way, from years to million-year time scales driven by Earth's orbital processes and rare aberrant shift and extreme climate transients during the last* 10^3 *to* 10^5 *years*". See page 1, line 22-23 in the revised manuscript.

1/35: "equivalent diffusion temperature that is always higher than the actual mean temperature" This statement, while true, gives the false impression that this is an intractable bias. For a system with well-characterised diffusion kinetics, the relationship between a given temperature history (e.g., a forward model) and the EDT is well known. In other words, paleothermometry using the He-3 paleothermometry technique must rely upon comparisons against prescribed temperature histories in the same way as paleothermometry with luminescence techniques. This is not a comparative disadvantage of the noble gas technique, but a similar limitation as faced in the current study.

This is true. We meant that a single thermometric system (OSL or ^{3}He) will always provide a single equivalent temperature (like EDT in ^{3}He) for a complex thermal history whereas a multi thermometric

system (here TL) with different temperature and time sensitivities will have the potential to infer a more complex thermal history. We have clarified the sentences to "*Tremblay et al. (2014a, b) recently introduced a new paleotemperature proxy based on the thermal stability and release of ^{3}He and ^{21}Ne noble gases in quartz. The system has a single energy level and is therefore only able to estimate a single equivalent diffusion temperature (EDT). As a result, reconstruction of complex rock temperature histories challenging.*" See page 1, line 33-36 in the revised manuscript.

2/6: The distinction between thermochronology and paleothermometry is not entirely clear in the language of this study. If what you aim to resolve is the temporal variation of temperature through time, you are describing thermochronology. If instead, you mean to resolve a past temperature which is representative of some time period (the measurement of which will be affected by seasonal variability and so on), then what you are describing is paleothermometry. I would encourage more precision when you describe these concepts.

Paleothermometry is a methodology for determining past temperature, and thermochronology is the study of the thermal evolution of rocks, and they both rely on the same principle. However, thermochronology is more commonly used for rock cooling related to exhumation. So to avoid confusion, we now use paleothermometry throughout the manuscript. We only refer to thermochronometry when we refer to previous work, which was developed for thermal evolution of rocks associated with exhumation.

2/12-21: Please add corresponding references for these observations.

Amended. See page 2, line 21 in the revised manuscript.

2/36ff: The physical meaning of this model is unclear. This is obviously of fundamental importance, as the kinetic model that is chosen will determine all predictions of past thermal history.

From Eq. 1, it would seem that the authors expect to model some number of individual traps, each with a singular values for D0, E, s, s-tilde, rho', a, and b. All of these traps are modelled as disconnected.

And yet, the transition in parameter values from one measurement temperature bin to another is smooth. This is true for D0, for rho', for E, for s, and for b within Fig. 1. This observation strongly suggests continuity in the underlying kinetics, not only for trap depth(s) but for the system as a whole. To fit each measurement bin as a separate and disconnected trap seems suspect. A unified treatment would be preferable.

Several studies suggest that broad TL glow curve from feldspar arises from a continuous distribution of trapping energies, which is suggested by several methods, like T_m-T_{stop}, the initial rise method, and analysis of fractional glow curves (Biswas et al., 2018; Duller, 1997; Grün and Packman, 1994; Pagonis et al., 2014; Strickertsson, 1985). Regardless, it is difficult to isolate a single trap with distinct kinetic parameters. Instead we assign the most probable kinetic parameters for each thermometer (glow curve temperature) along the TL glow curve and in this manner we determine kinetic values in a continuous, rather than in a disconnected manner. This is the method that we have adopted here and in Biswas et al.

(2018). We then arbitrarily choose 10 °C TL temperature windows as distinct thermometers. A continuous distribution of trapping energies can be assumed as the sum of a large number of discrete traps (Pagonis et al. 2014). Thus a continuous distribution of trapping energies is discretized as shown in the figure below. This has been added in the supplementary materials (section S1.2).

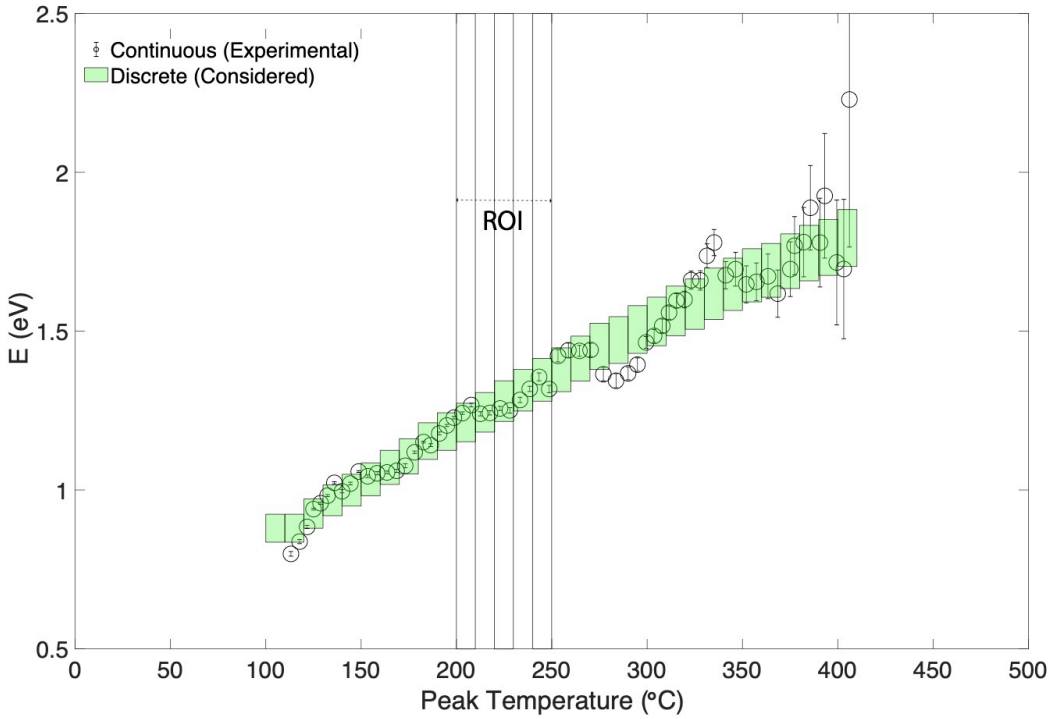

Fig. S1: The evaluated continuous distribution of trap depth (E) of sample MBTP1 (circles with error bar) and its discretization in 10 °C windows (green box; width is 10 °C and height 5 % of the median value).

Another issue to address is whether the same recombination centers are accessed by this distribution of traps during athermal fading. If so, as would seem unavoidable to some degree, rho should be kept constant (the density of centers being a property of the material). rho' can then be related to the underlying activation energy via the alpha term. This should be attempted for internal consistency.

Here we only use ρ', which includes alpha as $\rho' = \frac{4\pi\rho}{3\alpha^3}$. Alpha controls the rate of fading through the lifetime $\tau = s^{-1}\exp(\alpha r)$. It is expected that with increasing activation energy fading rate (ρ') should decreases as the tunnelling depth increases. Indeed we get similar relationship between fading rate (ρ') and activation energy (Table 1) as shown in figure below.

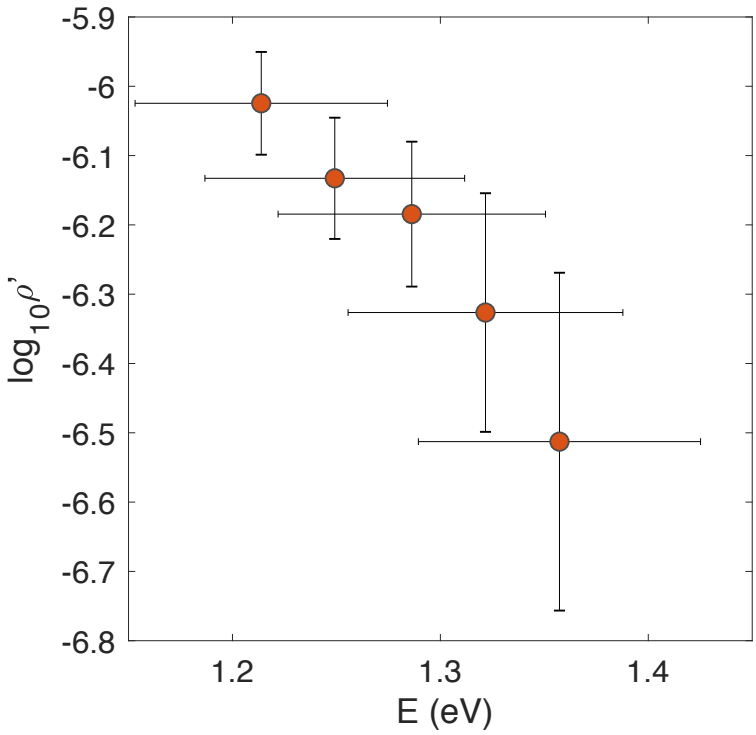

Fig. X: Plot of distance dependent fading rate (ρ') and activation energy (E) of five thermometers (200-250 °C, 10 °C interval) of sample MBTP9.

According to the second term on the RHS of Eq. 1, it seems that the authors model thermally-activated recombination locally (since the term is dependent upon the nearest neighbor distribution). If so, then observations of signal loss at room temperature could also be caused by this pathway. This deserves comment.

Thermal loss of the TL signals which is a more diffusive process (athermal) can occur through the conduction band. However, the power term b, accounts for the nonlinearity (delayed) arise due to presence of band-tail states. However, athermal fading is known as a tunnelling process. Separate treatments of thermal and athermal loss has adopted successfully in several previous studies (Guralnik et al. 2015a for IRSL of feldspar; Biswas et al. 2018 for TL of feldspar).

3/29-30: Can we be confident that the kinetic parameters pertain to geologic timescales? Specifically, is there good evidence or reason to think that mixed order kinetics are predicted at low temperatures and long timescales (natural) as well as high temperatures and short timescales (lab)? Competition effects, for example, could easily produce observations of b > 1 for lab measurements whereas the concentration of charge activated on natural timescales would be orders of magnitude smaller.

This is a difficult question and can never be answered in true sense but the premises of the approach used here was validated in Biswas et al. (2018), by successful recovering temperatures experienced by rocks in the KTB borehole, which have been in thermal steady state for several millions of years. We have included that statement in the manuscript.

4/19 and Fig. 3: I find this figure a little difficult to interpret. In particular, the way that you have defined 'memory time' should be a bit clearer. If I've understood the meaning of this metric correctly, one suggestion would be to compare everything against 'tchange = 100ka' or to extend the x-axis to include 't-change=150ka.' By doing this, you could then visually show the meaning of the 't-memory' by comparing two horizontal lines, one at t-change=150ka (or 100ka, depending), and the other at the asterisk height. You could then annotate this difference as 20%.

Amended as recommended. In the figure the 20% changes have been demonstrated clearly and text has been added in the figure title (Fig. 3).

It would be good to consider also the influence of measurement uncertainty. Accurately resolving the difference between [n-bar] = 2.0e-3 and 2.4e-3 would likely involve a lot more relative uncertainty than discerning between, say, [n-bar] = 0.5 and 0.6.

Typical photon counts of the present sample for near saturation ($\bar{n} = 1$) is $>10^5$ counts per second (cps), our instrumentation can resolve a few hundreds of cps with 20% uncertainty ($\bar{n}$ of the order of 10^{-3}). This is discussed in Section 4.3 (Page 8, line 23-26) as "*Typically, the minimum detectable limit for the present instrument is ~ 300 photon counts per second (cps) considering the signal should be three times of background level which is ~ 100 cps. The present highly luminescent feldspar has maximum photon count of ~10^6 cps. This restrict to use the TL signals up to ~10^{-3} % of maximum TL signals*"

4/30-31: '10 - 100 kyr timescales' This should be a bit more specific. During the Quaternary, the 100kyr and 41kyr periods were most dominant (e.g., Raymo et al., 2006; Hinnov, 2013).

We have changed the sentence to "*Earth's climate varies in cyclical way, at multiple time scales from years to decades, centuries, and millennia, influenced by periodic variations in the Earth's orbit, known as Milankovitch cycles, at 25.77, 41 and 100 kyr*". See page 4, line 30-31 in the revised manuscript.

Fig. 4: This is a nice figure. Please adjust so that the 'thermometer' labels correspond to each panel. For example, in panels j-l, if the reader uses the labels on the far righthand side, they might conclude that the bottom-most series in panel k refers to the 220-230C chronometer.

Thanks. Amended as recommended (Fig. 4).

5/7: 'implies a gradient' I would say this behavior more accurately 'results' from a gradient in thermal stability, given that the kinetic parameters are imposed and known.

Amended.

5/9: 'the thermal stability decreases with increasing temperature.' I disagree with this statement. The thermal stability for a given TL thermometer is known and fixed in your setup. So it is not the stability that is changing, but rather the probability of detrapping.

Thanks for pointing this out. The sentence has been reworded to "*This is because the probability of detrapping increases with increasing temperature*". See page 5, line 7 in the revised manuscript.

5/10: 'the higher temperature TL thermometers remain relatively insensitive to such periodic temperature forcing.' This is misleading. The insensitivity of the higher-T thermometers reflects the mean temperature values that you have chosen. If the temperature oscillated about a higher mean value, the same periodic filling/emptying behavior would be seen with the high-T thermometers. This is evident in Fig. 4 panels j-l, where different thermometers oscillate with comparable magnitude when a range of mean temperatures are tested.

The sentence has been changed to "*Finally, the higher temperature TL thermometers (near to 300 °C) remain relatively insensitive to such periodic temperature forcing (T_{mean} up to 30 °C); with increasing T_{mean} the higher temperature TL thermometers become more responsive.*". See page 5, line 7-9 in the revised manuscript.

5/13: '10 ka to 1 Ba' If Ba represents 'billion years,' please change to 'Ga.'

Amended.

5/15: 'For P « tau' This comparison must be qualified. The lifetime (tau) will depend on a chosen, singular temperature value. Choosing a singular temperature value for oscillating temperature requires some simplification that is not described (e.g., mean temperature? EDT?). Please clarify this issue.

The sentence has been clarified to "*For $P << \tau$ (e.g. Fig. 4d where P=1 ka and τ spans ~10 ka to 1 Ga for the 200 to 300 °C TL thermometers for T_{mean}= 0 °C), the value of $\bar{n}_{osc}$ exhibits small fluctuations but always remains lower than $\bar{n}_{iso}$*". See page 5, line 14-16 in the revised manuscript.

5/16: 'This result implies that smaller periods (<1 ka) do not influence trapped charge equilibrium levels in an oscillating fashion and cannot be differentiated from the trapped charge population resulting from an isothermal condition.'

This statement is incomplete and only conditionally true. For argument's sake, assume that the 200C TL thermometer has a lifetime of 10 ka at 0C. If the ambient temperature oscillated with an arbitrarily large amplitude (say 100C to make the point obvious) but with a period of only 1 ka or 100 yr, you would find that the fractional saturation would oscillate in response to the temperature forcing, depleting completely and then partially regenerating.

This won't happen if the temperature period is much smaller than the growth timescale (D0/Ddot). If that is the case, then the thermal imprint upon the sample approaches a steady value determined by the maximum temperature experienced.

Temperature amplitude and the relationship between the forcing period and sample growth timescale both matter. To make this comparison between lifetime and period, these factors must be incorporated.

The sentence has been modified to "*This result implies that smaller periods (<1 kyr) and Tmean (<30 °C) do not influence trapped charge equilibrium levels of 200 to 300 °C TL thermometers in an oscillating fashion and cannot be differentiated from the trapped charge population resulting from an isothermal condition. We must mention here, if the amplitude of oscillation increases the oscillating*

response to trapped charge equilibrium levels will be relatively prominent.". See page 5, line 16-19 in the revised manuscript. The effect of oscillating parameters, mean temperature, amplitude of oscillation and period on trapped charge population is discussed is section 2.2.2 (Page 5, line 28-35) and shown in Fig. 5.

5/19: 'remains correlated' and 'deviates from...temperature forcing' The meanings of these statements are unclear. n-bar behavior is distinct between isothermal and oscillating temperature histories for all periods; it is not an issue of matching and not matching, except for the highest-temperature systems, which are insensitive to the temperatures prescribed here. Please be more specific with these observations and, following from the previous comment, please do incorporate growth timescales, as these are of obvious relevance here.

Clarifications have been made. The sentence has been changed to "*Similarly, the present day* $\bar{n}_{osc}$ *remains indistinguishable from* $\bar{n}_{iso}$ *when* $P >> \tau$ *(e.g. see the behaviour of the low temperature TL thermometer shown in Fig. 4l)*". See page 5, line 21-22 in the revised manuscript.

5/24: 'Therefore, temperature variations can be reconstructed...' Just to reiterate, you must demonstrate the complex relationship among mean temperature, temperature amplitude, trap stability and regenerative timescales before attempting to reconstruct temperature variability. Additionally, what has been shown in Fig. 4 is that, for a given amplitude, different periods leave different imprints upon the shown thermometers. You have not yet demonstrated that you can accurately reconstruct differences in variability. Moreover, the results from Fig. 5 (panels b, c) seem to indicate that you cannot easily differentiate between various amplitudes or periods.

This is discussed in section 2.2.2 and Fig. 5 where we show that the present day trapped charge population ($\bar{n}_{present}$) is highly sensitive to the mean temperature (T_{mean}) and less sensitive to the amplitude of oscillation (T_{amp}) and period (P). Moreover, we also mention that "*Although the* $\bar{n}_{present}$ *is less sensitive to the amplitude and the period, the pattern of* $\bar{n}_{present}$ *of different thermometers is unique. This ensures that complex thermal histories comprising mutiple harmonics with periods of about tens of kyr, but distinct from one another, can be recontructed*". See page 5, line 32-35 in the revised manuscript. Additionally, now we have added a new synthetic test to emphasis the sensitivity of the three periodic parameter (T_{mean}, T_{amp} and P) on the present day trapped charge population ($\bar{n}_{present}$) in section 3.3 and results are shown in Fig. 6.

5/31-33: 'This ensures that complex thermal histories...can be reconstructed.' Following from the previous comment, this is not yet demonstrated.

See the answer above.

6/11: 'considering that the other parameters are identical.' Unclear what this means. From Fig. 1, it would seem that the kinetic parameters other than the thermal parameters (E, s) vary between the thermometers. Or do you mean something else?

We agree this was confusing. We have now removed these unnecessary words.

Fig. 7: This is not the most informative way to show your predictive ability. Unlike with thermochronology studies, where the T-t path is really the predicted feature, what you are more accurately doing is predicting the temperature minimum and amplitude (e.g., ll. 5/24-29). So, it would be much more informative to see these values, actual and predicted.

It is true that the only difference with the inversion of thermochronometric data is that we impose the shape of $\delta^{18}O$. To address the reviewer's comment we have added histograms of the two main scaling parameters: the minimum temperature T_{base} (temperature at 20 ka) and the present temperature, $T_{present}$ (which is $T_{base}+T_{amp}$ as shown in supplement Eq. S9). See Fig. 7.

Additionally, the current figure makes it appear as if you are able to resolve the fine structure of the T-t series, which of course you are not.

Indeed, we cannot. Rather this figure shows the scaling of the $\delta^{18}O$ curve. The reply to the previous comment should have addressed this comment.

7/16-18: '[Fig. 7a,b,c shows] it is possible to recover all three thermal histories within the 1-sigma confidence level.' My previous comment will apply here as well. What matters for this experiment is the degree to which you are able to predict amplitude and minimum.

To demonstrate that you could recover an arbitrary thermal history well, you would need a different test.

Please see the reply of previous comment. We clearly mention we need prior information for the pattern of the thermal history ($\delta^{18}O$), as typically done for inversions, but that we can constrain the temperature minimum and amplitude. Please see section 3.3 and 3.4 in the revised manuscript.

8/7: 'This restrict...' Grammar

Amended.

8/15: This dose range, with upper doses at 0.9 and 1.9 kGy may not be sufficient to observe saturation in K-feldspar TL. Please demonstrate that these signals are saturating or add greater doses to better constrain lab saturation intensity.

1.9 kGy is sufficiently high as it is greater than $2D_0$; maximum D_0 is less than 800 Gy (see Table 1).

8/33: 'no effect for doses below 100 Gy' Wouldn't the far more important question be whether there is sensitivity change above 100 Gy? After all, the majority of given doses are above 100 Gy and these responses allow you to determine the saturation values.

The sensitivity change in the NCF method permits determination of the equivalent dose correctly by correcting for possible sensitivity changes during a sample read out and is generally tested on low doses (see Singhvi et al. 2011).

9/13-15: 'The rationale here is that all temperatures follow the delta O-18 data, but the amplitude...and mean temperature are unknown.' Please make clear that this is a stated assumption and not an inference from studies (unless it is, in which case state that). I think is not obvious that the climate signal on Mont Blanc would mirror a Greenland ice core signal, so this assumption probably warrants justification.

To clarify, the text has been modified as follows "*We assume that the atmospheric temperatures of the Mont Blanc massif followed the trend observed for the Greenland ice core data over the last 60 ka. Note that temperature increase during the last glacial cycle was synchronous with the temperature anomalies observed in Greenland (e.g., Heiri et al., 2014; Schwander et al., 2000; van Raden et al. 2013). The rationale here is that all temperatures in the Mont Blanc massif follow the Greenland ice core δ18O data but the amplitude of temperature oscillation (minimum temperature at ~20 ka to maximum temperature at the present day) and mean temperature are unknown.*". See page 9 line 31-36 in the revised manuscript.

Fig. 9: Is Fig. 9 referenced in the main text?

Now it is mentioned.

Fig. 9 and 10: As with Fig. 7, please recast to compare the predicted and actual values for the amplitude and base temperatures as these are the variables being investigated.

We have now added subplots (histograms) of the two parameters, temperature minimum which we define as T_{base} (temperature at 20 ka) and present temperature, $T_{present}$ (which is $T_{base}+T_{amp}$ as shown in supplement Eq. S9). See Fig. 9 and 10.

9/28: 'can constrain thermal history of ~50kyr.' I do not think this has been demonstrated yet, as an extension of my comments regarding pg. 5.

In Fig. 3 we show that t_{memory} can be up to 50 kyr for typical temperature of 10-20 °C. If the amplitude of temperature change is higher, the method will be sensitive, thereby improving our ability to constrain the thermal history constraining of thermal history will be more precise. See section 2.2.1.

Also, unclear what 'A higher temperature fluctuation' means and whether you've actually shown this.

This is shown in Fig. 3.

10/14: 'At those depths [of 7 and 62 cm], mean temperature should be constant.' Certainly, there will be seasonal temperature variability at a depth of 7 cm. Is this what you meant to say?

We mean that at depths of 7 and 62 cm the rock temperature will be equilibrium with the atmospheric temperature. The sentence has been modified to "*At those depths, mean temperature should be in equilibrium with atmospheric temperature (e.g. Hasler et al. 2011)*" . See page 11, line 10-11 in the revised manuscript.

10/17: For inverse modeling of a natural sample, the time-temperature histories were completely random' If I have understood the previous text correctly, the histories are very much not random, but are tied to the Greenland delta O-18 temperature proxy with variability only in amplitude and initial temperature. Please reword.

The sentence has been reworded to "*For the inverse modeling of natural samples, $\delta^{18}O$ data are used as a prior on the shape of the thermal histories, but we leave two scaling parameters free – minimum temperature at 20 ka, and amplitude (temperature difference between at 20 ka and present)– and we did not include the role of ice on setting the rock temperature during glaciation.*". See page 11, line 13-15 in the revised manuscript.

Discussions generally: I won't comment much on these inferences about past climate systems at this stage, because I think it will be very important to first demonstrate model success in capturing simple variations within a periodic forcing model, which, at this stage, has not been done.

Anonymous Referee #2

This manuscript proposes a new method to study/reconstruct paleo-temperature using TL of feldspar from rock surface. Reconstructing paleo-temperature is an important topic in climatic change study, so the attempt of this study is important and worth for publication. However, there are some technical issues that are not settled well, which prevents convincing me that this is achievable. Here I summarise my major concerns.

1) Kinetic model: the authors considered three processes in their model, including dosing (growth), thermal decay and athermal decay (fading), which are represented by different terms in their equation 1. They then estimated the parameters based on TL measurements in different ways. For both the growth curve parameters (D0 and a) and fading parameters (rho'), my understanding is that they were based on the signals from different integrals of the TL glow curve (e.g., 200 – 250 C in 10C interval). However, for the thermal decay parameters (E, s and b), they used a Tm-Tstop method, in which the signal from each temperature interval is obtained from subtracting consecutive fractional glow curve. That means, the signals they used to estimate present-day charge population ($\bar{n}$), growth curve and fading are based on simple integral of TL signals at different intervals, which obviously are a mix of signals from a range of trapping energy levels, but the thermal kinetic parameters are based on single (or narrow-range) trapping energy levels. That says, the authors did not separate the TL signals for constructing their model using a similar way (Tm-Tstop method) that they did for estimating the thermal decay parameters. This is problematic, as the combination of different trapping levels are not linear, so their model (equation 1) simply becomes invalid when the signals being analysed are associated with a range of trapping levels are analysed. One need to makes sure that the different parameters in Equation 1 are all obtained from the same signal associated to a single or narrow-range energy level. I am not use if this can be achieved as the combination of MAR protocol (and fading test) and Tm-Tstop would be very difficult to achieve.

We do not assume that the thermal kinetic parameters are estimated on single trapping energy levels, as the number of traps are not known. In the absence of any information of the number of peaks it difficult to deconvolve the TL glow curve. So instead we use a 10 °C window and treat them as different 'thermometers', rather than single trapping energy levels. (Note that the rationale behind choosing a 10 °C window is the uncertainty of sample temperature during TL measurement in the laboratory.)

We constrain the growth parameters (D_0 and a) and fading parameter (ρ') for these different 10 °C temperature windows. To evaluate the thermal decay parameters (E, s, b) of each 'thermometer', we need to know the distribution of these parameters along the TL glow curve and find the most probable decay parameters of different thermometers from the distributions. Pagonis et al. (2014) demonstrated that the distribution of thermal decay parameters along a TL glow curve can be obtained using the *Tm-Tstop* method, subtracting the fractional glow curve and fitting with a TL equation. Biswas et al. (2018) adopted this method for thermochronology and showed it could be used to extrapolate laboratory data to geological timescales, as a proof-of-concept.

The subtraction of consecutive fractional TL glow curves, obtained through the *Tm-Tstop* method, and fitting of the subpeak provides the characteristics (kinetic parameters) at that TL temperature. The

integrated TL signal is a mix of different signals but the major contribution comes from the subpeak at that temperature range and a small fraction from the subpeaks either side of the temperature. Biswas et al. (2018) demonstrated (Fig. S4 in their supplement) that the life time distribution along the TL glow curve (present method) exactly match with classical lifetimes of the main dosimetric peaks of feldspar (as summarised in Aitken's TL book, 1985, Table E.1). This ensures the estimation of kinetic parameters of integrated TL signals from a distribution holds well.

Since last six to seven years there are lot of development on kinetic of luminescence of feldspar. The theoretical model for the rate equation of trapped charge population in feldspar has been described in several ways; first order kinetics (Brown and Rhodes, 2017; Yukihara et al., 2018), general order kinetics (Biswas et al., 2018; Guralnik et al., 2015b), charge transport through sub-conduction band-tail states (King et al., 2016a; Li and Li, 2013), Gausian distribution of trapped energies (Lambert et al., In Revision), or localized recombination in randomly distributed defects (Jain et al., 2012). What is common to all these models is that luminescence of feldspar is complicated and exhibit a non-linear non-first order kind of behaviour due to either presence of sub-conduction band-tail states (Morthekai et al., 2019; Poolton et al., 2002) or complex charge transport mechanism. TL in feldspar is even more complicated because it shows continuous distribution of trapping energies (Biswas et al., 2018; Duller, 1997; Grün and Packman, 1994; Pagonis et al., 2014; Strickertsson, 1985) and TL is a more diffusive process than OSL; OSL of feldspar has resonant energy levels (Hütt et al., 1988). Different models were reviewed and tested by Guralnik et al. (2015b) who suggested that the general order kinetic, a mathematically simplified model, could be used to explain luminescence phenomenon well. We adopted this model for TL of feldspar where the power terms (a, b) accounts for the nonlinearity involved in the TL of feldspar. The efficacy of using general order kinetics has been demonstrated to samples with known thermal history (KTB borehole samples) for OSL of feldspar (Guralnik et al., 2015a) and TL of feldspar (Biswas et al., 2018). This section has been added in the beginning of discussion section, page 10, line 7-19.

2) The authors simply assuming feldspar consist a continuous trapping energy level. However, it has been commonly accepted that band-tail states play important role in the luminescence process (including TL and IRSL) in feldspar (Poolton et al., 2002). I do not see any reason to discard the band-tail states from their model.

There is ample evidence from the literature suggesting that feldspar consists of continuous trapping energy levels (e.g. Biswas et al., 2018; Duller, 1997; Grün and Packman, 1994; Pagonis et al., 2014; Strickertsson, 1985).

We do not discard band-tail states in feldspar. See the reply of previous comment. Feldspar luminescence is complicated and several models that describe thermal detrapping processes in feldspar have been proposed (see summary in Gurlanik et al., 2015b). Moreover, the TL of feldspar is a more diffusive process than IRSL which excites a resonant energy level below conduction band from which electrons either tunnel to recombination centers or hop through the band-tail states and recombine. The general order kinetic model is the simplest model available and the power term b (>1) accounts for the non-linearity that arises due to the presence of the band tail states (restricted mobility) or other complex

process. This model has been used for a long time and most recently was used by Guralnik et al. (2015) for IRSL of feldspar and Biswas et al. (2018) for TL of feldspar.

3) How sensitive is the model to dose rate ($\dot{D}$)? The dose rate would play an important role in filling the traps during natural process, so I would expect that it will somehow influence the model results. Unfortunately, the dosimetry of the samples is poorly described. How did the author estimate the dose rate of K-feldspar? The author appears to simply crush the rock and select 150 –250 um grain size range. What are the original grain sizes of the K-feldspar minerals in the rock? Did the authors make any rock slide to investigate this? This is critical as there are a large contribution of internal dose rates for Kfeldspar.

The dose rate values were taken from Lehman et al. (2020). It is mentioned in title of Table 1. They mention in their paper (supplement) as follows: "Environmental dose rates were calculated using DRAC online calculator (Durcan et al., 2015), assuming a grain size between 750 and 1000 μm and water content of 2%". The grain sizes were estimated through thin section analysis by Lehman et al. (2020).

4) The authors applied the NCF method to overcome sensitivity change issue for TL measurements. They do realise the limitation of this method as it is based on extrapolation of the NCF values from low temperature to high temperature region, which is unreliable. Although the authors tested the effect of initial sensitivity changes on the modelling results and found very little changes for their sample, it does not guarantee that this applies to other samples and situations. The reason that the sensitivity changes did not affect the results is simply because that their samples are young and the growth of signal still lies on the linear part of growth curve, so any systematic changes in the sensitivity result in a proportional changes of different signal integrals. For older samples or high-De samples, however, this may result in non-proportional changes among different signal integrals (because the different D0 values for different integrals), and, hence, different model results in paleo-temperature. This potential problems should be appropriately acknowledged as at present it gives false impression that the initial sensitivity change does not matter.

We agree and have included appropriate caveats. Sensitivity change is a limitation for TL measurements and as such we carefully screened the data. As for all TL measurements this will need to be done in further studies but as this is well known we do not emphasise the point here, but rather give a detailed account of how we addressed this challenge.

To circumvent the initial sensitivity change the NCF was introduced (Singhvi et al. 2011) as shown in Fig. 8a. The limitation of this method is that the NCF can only be measured for the lower temperature part of the TL signal (<200 °C) where our region of interest (ROI) is 210-250 °C TL. In the absence of a strong correlation (dose response) between low temperature TL and the ROI, we extrapolated. As the reviewer notes, this approach is appropriate for our sample suite. See section 4.3.1.

Minor comments:

5) Line 21: Credits should be given to Li and Li (Li and Li, 2012) who firstly proposed the idea of multiple-thermometers using TL (although not implemented in their study), and they also first

introduced the rate equation to investigate the effect of single growth and saturation on OSLthermochronology.

Reference added.

6) Figure 1: The authors should at least provide some typical TL glow curves for their samples before showing the kinetic results.

Amended.

7) Figure 1c: The fading parameter (rho') shows systematic change as a function of temperature up to 280C, but it suddenly become 'no fading'. This is surprising. The different integral signals represent a continuous mixture of signals of different athermal features, why one can obtain a sudden change in the fading? Is it because that the fading rate has large uncertainty range consistent with zero fading? In this case, it would be problematic to say 'no fading', as statistically it is also like to be 'fading'.

Beyond 270 °C, the fading parameter (ρ') is less than 10^{-10} with large uncertainty and is considered to be a non-fading signal. Even a fading curve with $\rho'<10^{-7}$ looks parallel to the time axis.

8) Figure 8b: Why not plot the results for other temperature range (e.g., 120 – 150 C)?

The objective is to see whether NCF_{100} is dose dependent or not.

9) Figure 8c: what are the errors for the NCF at high temperature range (200 – 250C)? Have you incorporated the NFC errors into the final results?

The errors for the NCF at the high temperature range (200 – 250 °C) are stated in Table 1. We did not incorporate NFC errors into the final results.

10) Table 1: Why there are no errors for E, s and b? Why an arbitrary error of 5% is assumed, rather than their actual analytical errors?

See Fig. 1. The distribution of E, s and b are a bit scattered and we spline fit the trend. So we did not calculate the regression of the trend and rather assumed an working error of 5%. This is mentioned in the caption of Table 1.

11) Figure S3: why there is only one natural point but 3 regenerative points for each thermometer? Did the author just measure one aliquot for natural?

The natural point is the average of three discs. This is mentioned in the title of Fig. S3.

List of corrections

1. We have addressed all the queries of the reviewers and incorporated them in the revised manuscript and actions taken are mentioned in the replies to the reviewers' comments.
2. Two major changes are made in the this revised version of manuscript, 1) we introduce a new synthetic experiment in section 3 to justify the rationale behind using the trend of $\delta^{18}O$ in the inverse modelling. 2) we have added a paragraph in the beginning of Discussion section to justify the model used.
3. All changes made in the manuscript can be seen in marked-up manuscript version (track change mode) attached herewith.

Surface paleothermometry using low temperature thermoluminescence of feldspar

Rabiul H. Biswas[1], Frédéric Herman[1], Georgina E. King[1], Benjamin Lehmann[1], Ashok K. Singhvi[2]

[1]Institute of Earth Surface Dynamics, University of Lausanne, Lausanne, Switzerland
[2]Atomic, Molecular and Optical Physics, Physical Research Laboratory, Ahmedabad, India
Correspondence to: Rabiul H. Biswas (biswasrabiul@gmail.com)

Abstract. Thermoluminescence (TL) of feldspar is investigated for its potential to extract temperature histories experienced by rocks exposed at Earth's surface. TL signals from feldspar observed in the laboratory arise from the release of trapped electrons from a continuous distribution of trapping energies that have range of thermal stabilities. The distribution of trapping energies, or thermal stabilities, is such that the lifetime of trapped electrons at room temperature ranges from less than a year to several billion years. Shorter lifetimes are associated with low temperature TL signals, or peaks, and longer lifetimes are associated with high temperature TL signals. Here we show that trapping energies associated with shorter lifetimes, or lower temperature TL signals (i.e., between 200 °C and 250 °C), are sensitive to temperature fluctuations occurring at Earth's surface over geological timescales. Furthermore, we show that it is possible to reconstruct past surface temperature histories in terrestrial settings by exploiting the continuous distribution of trapping energies. The potential of this method is first tested through theoretical experiments, in which a periodic temperature history is applied to a kinetic model that encapsulates the kinetic characteristics of TL-thermometry. We then use a Bayesian approach to invert TL measurements into temperature histories of rocks, assuming that past temperature variations follow climate variations observed in the $\delta^{18}O$ records. Finally, we test the approach on two samples collected at the Mer de Glace (Mont Blanc massif, European Alps) and find similar temperature histories for both samples. Our results show that TL of feldspar may be used as a paleo-thermometer.

1 Introduction

Earth's climate fluctuates in a cyclic way, from years to million-year time scales driven by Earth's orbital processes and rare aberrant shift and extreme climate transients during the last 10^3 to10^5 years (e.g., Zachos et al., 2001). Reconstructions of past terrestrial climates often rely on the use of climate proxies that preserve the physical and/or chemical characteristics related to past climate of Earth's history. Examples of such proxies include ice cores, tree rings, sub-fossil pollen, boreholes, corals, lake sediments and carbonate speleothems (e.g., Jones and Mann, 2004 for a review). Although they have provided invaluable insights into past climates and their physical characteristics, very few of these proxies provide a direct measure of temperature variations in continental settings (e.g., glycerol dialkyl glycerol tetraether, GDGT; Tierney et al., 2012), and many of these methods often suffer from methodological limitations that limit reliable construction of terrestrial temperatures. For example, fossil pollen and plant macrofossils have provided key insights into past terrestrial climate at millennial timescales (e.g., Bartlein et al., 2011), but typically rely on numerous additional climate parameters, including precipitation, plant-available moisture, seasonality, and the length of the growing season that make the inference of rock temperature histories challenging. Similarly, GDGTs rely on the preservation of organic compounds. To address some of these issues, Tremblay et al. (2014a, b) recently introduced a new paleotemperature proxy based on the thermal stability and release of ^{3}He and ^{21}Ne noble gases in quartz. The system has a single energy level and is therefore only able to estimate a single equivalent diffusion temperature (EDT). As a result, reconstruction of complex rock temperature histories challenging.

This study revives the use of thermoluminescence (TL) as a paleothermometer and takes advantage of recent progress made for TL thermochronometry (Biswas et al., 2018) to introduce a new approach for reconstructing temperature histories in

Deleted: the
Deleted: anomalies
Deleted: seasonal
Deleted: /
Deleted: also
Deleted: Although this new method shows great potential, the
Deleted: that is always higher than the actual mean temperature, and in turn makes the

terrestrial settings at millennial timescales. The idea is not new; it has already been tested through a series of feasibility studies (Li and Li, 2012; Ronca, 1964; Ronca and Zeller, 1965) and was applied to lunar samples (Durrani et al., 1977). Unfortunately, the method has remained underdeveloped since this early work. More recently, Guralnik and Sohbati (2019) used Optically Stimulated Luminescence (OSL) to estimate paleotemperature. However, they only investigated a single thermal stability, and thus a single equivalent temperature, similar to the noble gas approach of Tremblay et al. (2014a, b).

The present study aims to establish TL of feldspar as a paleothermometer to constrain temporal variations of Earth's surface temperature, within the last few tens of thousands of years. TL signals from feldspar arise from a series of traps that have different thermal stabilities; with lifetimes at room temperature ranging from <yr to >Gyr (Biswas et al., 2018). In the following, we first investigate the sensitivity of the TL signals to linear and periodic thermal histories. Then, we use a Bayesian approach to infer the thermal histories of rocks from TL measurements. Finally, we apply this method to two samples collected from the Mer de Glace glacier (Mont Blanc massif, European Alps) as proof-of-concept.

2 Theoretical background

In its simplest form, luminescence enables the measurement of the concentration of charge trapped in the impurity or defect centers of natural crystalline minerals (e.g., quartz or feldspar); the trapped charge population is proportional to the time elapsed since the material was either heated or exposed to sunlight. In the laboratory when the minerals are heated using a linear heating rate, trapped electrons are released from increasingly higher energy traps, some of which recombine radiatively with the holes, and the luminescence process generates a TL glow curve. Trapping of electrons happens in nature when samples are exposed to environmental radiation over geological time. Detrapping reflects the escape of electrons from traps, which can occur thermally or athermally. In nature, the TL system can reach a dynamic equilibrium between radiation induced growth and decay via thermal and athermal pathways. For higher ambient temperatures, the thermal decay rate is greater, which results in a lower equilibrium level and vice versa (for more details see Aitken, 1985 and Ronca, 1964). Such a difference in equilibrium can be exploited to reconstruct the thermal history of rocks (Biswas et al., 2018; Brown et al., 2017; Guralnik and Sohbati, 2019; Herman and King, 2018; Herman et al., 2010; King et al., 2016a; King et al., 2016b). Until now, this principle has only been exploited for inferring rock cooling due to exhumation. Here we use the same principle for inferring the paleotemperature of rocks exposed at Earth's surface. In this section, we start by outlining the theoretical model that describes the TL process of feldspar, and how can one constrain all the model parameters. Then we assess how sensitive the model is to various surface temperature histories and ultimately show how surface temperatures in terrestrial settings can influence TL signals.

2.1 TL kinetic model and TL thermometer

The kinetic model that describes TL of feldspar was reviewed in Biswas et al. (2018). The model encapsulates the process of populating traps with electrons in response to surrounding radiation, and the processes of electron escape through thermal and athermal pathways. A key element of the method is that each kinetic parameter can be constrained in the laboratory for each sample. We briefly outline the kinetic model here and illustrate how the kinetic parameters may be constrained from laboratory measurements for one sample. The reader is referred to the supplementary material S1 and Biswas et al. (2018) for further information.

The model assumes general order kinetics (Biswas et al., 2018; Guralnik et al., 2015a; Guralnik et al., 2015b). The rate equation for the trapped charge population of a specific trapping center, with single trap depth (E), frequency factor (s), and athermal fading parameter (ρ'; Huntley, 2006; Tachiya and Mozumder, 1974) is as follows:

Deleted: (
Deleted: ; Guralnik and Sohbati, 2019
Deleted: Byr
Deleted: with
Deleted: .
Deleted:).

$$\frac{d}{dt}\left(\bar{n}(r',t)\right) = \frac{\dot{D}}{D_0}\left(1-\bar{n}(r',t)\right)^a - se^{-\frac{E}{kT}}\left(\bar{n}(r',t)\right)^b - \tilde{s}e^{-\rho' r'^{-\frac{1}{3}}r'}\bar{n}(r',t) \quad (1)$$

where $\bar{n}$ is equal to n/N (where n is the number of trapped electrons at time t and temperature T, and N is the total number of available traps), $\dot{D}$ is the dose rate due to ambient radioactivity (Gy ka^{-1}), D_0 is the onset of dose saturation (Gy), a and b are the kinetic orders of trapping and thermal detrapping respectively, E is the trap depth or activation energy (eV), s and $\tilde{s}$ are the thermal and athermal frequency factor respectively (s^{-1}), ρ' is the dimensionless athermal fading rate and r' is a dimensionless distance that characterizes the probability of athermal escape (Huntley, 2006). Each of these parameters can then be constrained from laboratory experiments that are described in Biswas et al. (2018) and summarized in the supplementary material S1 for one sample.

To account for athermal loss, i.e., anomalous fading (Wintle, 1973), the total number of trapped electrons at any instant $\bar{n}(t)$ is obtained by integrating over the whole range of dimensionless distances ($0< r' <2$; Kars et al., 2008) over which electrons can athermally escape;

$$\bar{n}(t) = \int_0^\infty p(r')\bar{n}(r',t)dr' \quad (2)$$

where $p(r')$ is the probability of nearest recombination center at a distance between r' and $r'+dr'$ and expressed as $p(r')dr' = 3r'^2e^{r'^3}dr'$ (Huntley, 2006). This model was validated using rocks from the KTB borehole and applied to samples from Namche Barwa (Biswas et al., 2018), which gave results in agreement with other studies from the same area (King et al., 2016a).

TL of feldspar arises from a continuous distribution of trapping energies (Biswas et al., 2018; Duller, 1997; Grün and Packman, 1994; Pagonis et al., 2014; Strickertsson, 1985) and can be assumed as sum of a large number of traps (Biswas et al., 2018; Pagonis et al., 2014); all follow the process described by Eq. 1. To constrain the kinetic parameters in Eq. 1, we measure full TL glow curves and see how the kinetic parameters are distributed along the TL glow curve (Biswas et al., 2018). For the modeling, we use the kinetic parameters for sample MBTP9 (Lehmann et al., 2020 for sample details). The experimental details are provided in section 4 and supplementary material S1. The distribution of kinetic parameters along the TL glow curve temperature is reported in Fig. 1. The results show that the kinetic parameters vary systemically with the glow curve temperature. Such data are then fitted using a spline function from which the kinetic parameters are then extracted for a specific TL temperature (Biswas et al., 2018), which we define herein as a specific "TL thermometer".

Figure 1

2.2 Temperature response of TL thermometers

In this section, we use the model (Eq. 1) in a forward manner by prescribing a temperature history and predicting the trapped charge population through time ($\bar{n}$). Both linear (isothermal, warming and cooling) and periodic thermal histories are used. The model was run for 1 Myr, with an initial condition of $\bar{n}$=0, which is long enough to ensure that $\bar{n}$ reaches equilibrium. We investigate how $\bar{n}$ changes for ten different TL thermometers, in the temperature range of 200-300 °C with 10 °C intervals, each having an independent set of kinetic parameters (see the supplement Table S1).

2.2.1 Linear thermal history

The thermal response of the dynamic equilibrium level of the trapped charge population ($\bar{n}$) of the ten thermometers is tested for three different linear thermal histories: 1) isothermal holding at 20 °C (Fig. 2a), 2) isothermal holding at 20 °C for 900 kyr

Deleted:

Deleted: a

Deleted: To infer the kinetic parameters, we assume here that

Deleted: trap

Deleted: that the TL process is reflected by the

Deleted: growth

Deleted: (Biswas et al., 2018)

Deleted: .

Deleted: 2019b

Deleted: with

Deleted: Thermal

followed by linear cooling to 0 °C during the last 100 kyr (Fig. 2b), and 3) isothermal holding at 0 °C for 900 kyr followed by linear heating to 20 °C during the last 100 kyr (Fig. 2c). The results are shown in Fig. 2d, e and f respectively. In all cases, $\bar{n}$ is lowest for the lowest TL thermometers (or TL signals) and highest for the highest TL thermometers. For the isothermal scenario, $\bar{n}$ remains constant over the entire recent time (after reaching steady state) as there is no temperature change. For the cooling scenario, $\bar{n}$ increases as temperature decreases, because of a decrease of thermal loss. For the warming scenario, $\bar{n}$ decreases as temperature increases because of an increase of thermal loss. The increase and decrease of $\bar{n}$ (Figs. 2d and e) with temperature are most pronounced for lower temperature TL thermometers (<250 °C) and negligible for higher temperature TL thermometers (>250 °C). It must be noted that if the amplitude of temperature change (here 20 °C) were increased, the higher TL thermometers would change more dramatically. However, this would be unrealistic and beyond temperature variations observed at Earth's surface at comparable timescales.

Figure 2

The previous section shows that the thermal sensitivities of the different TL thermometers are distinct. It is therefore expected that their temporal sensitivities are also different. To quantify the temporal response of each TL thermometer, we prescribe a simple step function in which the temperature is set equal to 0 °C until a given time, t_{change}, and then increases to 10, 20 and 30 °C, in three different cases. We then calculate the present day trapped charge population ($\bar{n}_{present}$) for each TL thermometer. t_{change} is varied from 100 kyr to the present.

The model predictions ($\bar{n}_{present}$) are shown as a function of time of change (t_{change}) in Fig. 3. In addition, we calculate the t_{change} where $\bar{n}_{present}$ increases by 20 % compared to $\bar{n}_{present}$ predicted for a thermal history where t_{change} is equal to 100 kyr. We define this corresponding time as the memory time (t_{memory}) at which the TL thermometer can record a temperature change. As expected, the lower TL thermometers record more recent temperature changes and the higher TL thermometer record older temperature changes. For example, in case of a 10 °C temperature change (Fig. 3a), the 200-210 °C thermometers record a change for ~10 kyr, while the 240-250 °C thermometers record a change for ~50 kyr. Furthermore, the number of sensitive thermometers increases as we raise the final temperature. For a 10 °C temperature change, only 5 TL thermometers (200-250 °C) record the temperature change (Fig. 3a), 6 TL thermometers (200-250 °C) record a 20 °C temperature change (Fig. 3b), and 7 TL thermometers (200-250 °C) record a 30 °C temperature change (Fig. 3c).

Figure 3

2.2.2 Periodic thermal history

Earth's climate varies in cyclical way, at multiple time scales from years to decades, centuries, and millennia, influenced by periodic variations in the Earth's orbit, known as Milankovitch cycles, at 25,77, 41 and 100 kyr. Therefore, temperatures are dictated by periodic functions that include several harmonics comprising decadal and millenial periods. In order to assess how the trapped charge population is affected by a periodic temperature history, we prescibe the following function as a thermal history.

$$T(t) = T_{mean} + T_{amp} \times \sin\left(\frac{2\pi}{P}t\right) \quad (3)$$

where T_{mean}, T_{amp}, and P are the mean temperature, the amplitude, and the period of oscillation respectively.

Different combinations of arbitrary periodic thermal histories, with the same amplitude (10 °C), but three different periods (1, 10, 100 kyr) and three different mean temperatures (0, 15 and 30 °C) were used (solid lines of Fig. 4a,b and c) to assess the

Deleted: over
Deleted: over
Deleted: degree
Deleted: ka
Deleted: ka
Deleted: the
Deleted: In nature,
Deleted: on a daily
Deleted: seasonal basis and follows
Deleted: 10 to
Deleted: timescales
Deleted: seasonal to
Deleted: ka

effect of periodic temperature variations on $\bar{n}$ ($\bar{n}_{osc}$) for each TL thermometer (solid lines of Fig. 4d-l). These predictions are compared to isothermal effects on $\bar{n}$ ($\bar{n}_{iso}$) (dashed line in Fig. 4d-l) if the samples are kept at the mean temperature of the corresponding oscillation (dashed lines of Fig. 4a,b and c).

The results show that the $\bar{n}$ always depletes more for the lower temperature TL thermometer (e.g., 200-210 °C TL) than for the higher temperature TL thermometer (e.g., 290-300 °C TL), which results from a gradient in the thermal stabilities of lower to higher temperature TL thermometers. For every TL thermometer, $\bar{n}$ decreases if the mean temperature, T_{mean}, increases (Fig. 4d-f, g-i and j-l). This is because the probability of detrapping increases with increasing temperature. Finally, the higher temperature TL thermometers (near to 300 °C) remain relatively insensitive to such periodic temperature forcing (T_{mean} up to 30 °C); with increasing T_{mean} the higher temperature TL thermometers become more responsive.

Figure 4

One can also describe how the system behaves by comparing the period of oscillation (P) and the lifetime (or resident time) of trapped electrons (τ) for a given temperature. For the 200 to 300 °C TL thermometers, τ spans ~10 kyr to 1 Gyr when the samples are at 0 °C; at higher temperatures τ is reduced as the probability of electron escape increases, reducing the lifetime to between ~0.1 kyr and 1 Myr when the samples are stored at 30 °C (Biswas et al., 2018). For P<< τ (e.g. Fig. 4d where P=1 kyr and τ spans ~10 kyr to 1 Gyr for the 200 to 300 °C TL thermometers for T_{mean}= 0 °C), the value of $\bar{n}_{osc}$ exhibits small fluctuations but always remains lower than $\bar{n}_{iso}$. This result implies that smaller periods (<1 kyr) and T_{mean} (<30 °C) do not influence trapped charge equilibrium levels of 200 to 300 °C TL thermometers in an oscillating fashion and cannot be differentiated from the trapped charge population resulting from an isothermal condition. We must mention here, if the amplitude of oscillation increases the oscillating response to trapped charge equilibrium levels will be relatively prominent. However, the predicted values of $\bar{n}_{osc}$ are lower than those predicted using constant temperature of T_{mean}, which is the mean temperature of the oscillation explored. Similarly, the present day $\bar{n}_{osc}$ remains indistinguishable from $\bar{n}_{iso}$ when P>>τ (e.g. see the behaviour of the low temperature TL thermometer shown in Fig. 4l). These two end-member scenarios are therefore not suitable for predicting the temporal variation of surface temperature. Interestingly, the response of $\bar{n}_{osc}$ deviates from its temperature forcing when $P \sim \tau$ (e.g., Fig. 4g-i and j-l). Under this condition, $\bar{n}_{osc}$ is out of phase and asymetric compared to the prescribed forcing, i.e., the thermal history. More importantly, the degree of deviation for different thermochronometers is different. Therefore, temperature variations can be reconstructed by targeting TL thermometers that have lifetimes of trapped electrons comparable to the period of surface temperature changes.

As discussed in the previous section, the response of trapped electron concentrations corresponding to a TL thermometer depends highly on the three characteristic parameters of the periodic forcing, i.e., T_{mean}, T_{amp} and P. We now test the sensitivity of the model to these three parameters. The present day trapped charge population ($\bar{n}_{present}$) is predicted for different arbitrary combinations of T_{mean} (0, 15 and 30 °C), T_{amp} (5, 10 and 20 °C) and P (1, 10 and 100 kyr). The results show that $\bar{n}_{present}$ is highly dependent on the mean temperature variation, and less dependent on the amplitude and the period (Fig. 5). Although the $\bar{n}_{present}$ is less sensitive to the amplitude and the period, the pattern of $\bar{n}_{present}$ of different thermometers is unique. This ensures that complex thermal histories comprising mutiple harmonics with periods of about tens of kyr, but distinct from one another, can be recontructed.

Figure 5

Deleted:

Deleted: implies

Deleted: thermal stability decreases

Deleted:).

Deleted: ka

Deleted: Ba

Deleted: Ma

Moved (insertion) [1]

Deleted: ka

Deleted: ,

Deleted: (

Moved up [1]: Fig.

Deleted: 4d).

Deleted: ka

Deleted: equlibrium

Deleted: $\bar{n}_{iso}$

Deleted: temeprature

Deleted: correlated with $\bar{n}_{iso}$

Deleted: ka

Deleted: ~

3 Inversion of TL data into realistic thermal histories

The objective of this section is to test whether a temperature history can be recovered by inverting TL data into a realistic thermal history. We start the exercise by predicting TL data using Eq. 1 for a specific thermal history (forward modeling) that we then invert using a Bayesian approach (Biswas et al., 2018; King et al., 2016a; King et al., 2016b) (inverse modeling). This synthetic experiment is performed in two different cases. First, we describe the forward and inverse modeling in a general way and then report the two synthetic examples.

3.1 Forward modeling

Forward modelling is achieved by solving Eq. 1 and prescribing a thermal history, similarly to the previous sections. This approach enables us to predict the present day trapped charge population for a specific TL thermometer using the kinetic parameters extracted for sample MBTP9. Using this approach, we generate a range of "observed values" ($\bar{n}_{obs}$) for a particular thermal history, which we then try to recover using an inversion method. We run the model for 1 Ma to ensure that $\bar{n}$ reaches steady state assuming an initial condition of $\bar{n}$=0. For a specific thermal history, TL thermometers with lower thermal stability exhibit lower $\bar{n}_{obs}$ than TL thermometers with higher thermal stabilities. It is worth noting that the predicted $\bar{n}_{obs}$ values are mostly sensitive to two parameters, the trap depth (E) and athermal fading (ρ'), such that these must be constrained carefully from laboratory experiments.

3.2 Inverse modeling

To invert TL data ($\bar{n}_{obs}$) into a thermal history, a Bayesian approach is used. We first generate a large number of random thermal histories (300,000). For each random path, the present-day TL signals are predicted by solving Eq. 1. Each predicted present day TL values ($\bar{n}_{predict}$) is then compared with the observed TL ($\bar{n}_{obs}$) using the following misfit function (Wheelock et al., 2015) and likelihood:

$$misfit = \frac{1}{l}\sum_{i=1}^{l}\left[\frac{1}{2}\times\frac{\bar{n}_{obs}}{\sigma_{\bar{n}_{obs}}}\times\log\frac{\bar{n}_{predict}}{\bar{n}_{obs}}\right]^2 \quad (4)$$

$$likelihood = \exp(-misfit) \quad (5)$$

where l is the number of TL thermometers (here l=4) and $\sigma_{\bar{n}_{obs}}$ is the uncertainty of corresponding $\bar{n}_{obs}$. An arbitrary uncertainty of 20% of $\bar{n}_{obs}$ is assumed for synthetic test. For each random path $\bar{n}_{predict}$ for a specific thermometer is usually calculated using mean values of the specific set of kinetic parameters (Biswas et al., 2018; King et al., 2016a; King et al., 2016b). However, the kinetic parameters have uncertainties as shown in Fig. 1 and supplementary Table S1. To accommodate the measurement uncertainties in kinetic parameters, for each random thermal history, we randomly picked the kinetic parameters within its error range. Finally, $\bar{n}_{obs}$ was also randomly picked within its error range assuming that any value within error limit is equally probable (c.f. Guralnik et al., 2015). Since the randomization is applied to a large number of parameters, it is necessary to run the model for large number of thermal histories (300,000 iterations here).

The thermal histories that best fit the data are selected using a rejection algorithm that satisfies the criterion *likelihood* >R, where R is a random number between 0 and 1. A probability density distribution is then constructed by counting the number of accepted thermal histories passing through each grid cell, which is generated by dividing the time-temperature space (0-100 ka and -50 to 50 °C) into 100×100 cells. This approach is commonly used in different thermochronometric studies (Biswas et al., 2018; Braun et al., 2012; Gallagher et al., 2009; King et al., 2016b). It should be noted that the misfit function (Eq. 4) used here is different to the one used in previous studies (Biswas et al., 2018; King et al., 2016b) but is the same as that used in

Deleted:).

Deleted: prediction of

Deleted: ran

Deleted: , considering that the other parameters are identical.

Moved down [3]: For each thermal history, the present day trapped charge concentrations ($\bar{n}_{obs}$) are calculated for four TL

Moved down [4]: The results reported in Fig.

Deleted: Here we report the result of forward modelling of three thermal histories assuming that the temperature follows the measured δ^{18}O anomalies from Greenland for the past 60 kyr

Moved down [2]: , which is based on various records from the DYE-3, the GRIP, and the NorthGRIP ice cores (Svensson et al., 2008).

Moved down [5]: show a clear depletion of the trapped charge population during the last 20 kyr, for all investigated scenarios. However, high frequency temperature variations are dampened, implying that TL thermometry is insensitive to short term variations. This result is consistent with the results shown in Fig. 4.

Moved down [6]: *Figure 6*¶

Deleted: For our purpose, we scale the δ^{18}O anomalies to thermal histories and assume a constant temperature prior to 60 ka (Fig. 6a, b and c).

Deleted: thermometer (210-250 °C, 10 °C interval).¶

Deleted: 6d, e and f

Deleted: ¶

Moved down [7]:), which we scaled randomly by varying the amplitude of the temperature oscillation (i.e., the difference between minimum the temperature, which is at ~20 ka, and the maximum temperature at present) between 0 and 40 °C and the minimum temperature (i.e., temperature at ~20 ka) from -20 to 30 °C (

Deleted: supplement S2).

Moved down [8]: Note that making this assumption is somewhat equivalent to assuming a prior estimated on the inferred thermal history (Tarantola, 2005).

Deleted:) assuming that they all follow the ice core δ^{18}O Greenland anomalies (Svensson et al., 2008

Deleted: ¶

Deleted: were

Deleted: was

Deleted: .

Deleted:),

Deleted: was

Deleted: in the current study

King et al. (2019). We find that a log misfit enables us to better fit data that vary across orders of magnitude, as trapped charge populations vary greatly for different TL signals.

3.3 Synthetic approach 1

We choose three arbitrary periodic thermal histories, Path1 (T_{mean}= 10 °C, T_{amp}= 10 °C and P= 25.77 kyr), Path2 (T_{mean}= 20 °C, T_{amp}= 10 °C and P= 25.77 kyr) and Path3 (T_{mean}= 10 °C, T_{amp}= 20 °C and P= 25.77 kyr) as shown Fig. 6a. For each thermal history, the present day trapped charge concentrations ($\bar{n}_{obs}$) are calculated for four TL thermometers (210-250 °C, 10 °C interval) as described in section 3.1 and represented in Fig. 6b-d. We then invert the TL data ($\bar{n}_{obs}$) into a thermal history as described in section 3.2. For the inverse modelling, we first generate a large number of random periodic histories (300,000) with T_{mean} and T_{amp} randomly varying from 0 to 50 °C, P randomly varies between three cycles, 25.77, 41 and 100 kyr. We do not vary P in a completely random fashion because $\bar{n}_{obs}$ is less sensitive to P; i.e., it is difficult to resolve neighboring periods (as discussed in section 2.2.2 and Fig. 5). The results are shown in Fig. 6e-j. Although this approach predicts the very recent temperature well (up to max 5 ka) it loses the periodic information (25.77 kyr) because of the significant number of accepted thermal histories with different periods (41 and 100 kyr). The same exercise was repeated but fixing the period to 25.77 kyr for the inversion. The results are shown in Fig. 6k-p. Interestingly, this approach enables to recover the actual solution within 1σ uncertainty. This shows that a periodic thermal history can be predicted well if the period is known a priori; it enables to constrains T_{mean} and T_{amp} satisfactorily. To circumvent the limitation (period) of this method we use synthetic approach 2, the δ^{18}O data to impose the shape of the thermal histories as a priori information. This is typically done for inversion problem when appropriate. We then constrain T_{mean} and T_{amp} of the spectrum (as discussed in next section).

Figure 6

3.4 Synthetic approach 2

Here we report the result of three thermal histories assuming that the temperature follows the measured δ^{18}O records from Greenland for the past 60 ka, which is based on various records from the DYE-3, the GRIP, and the NorthGRIP ice cores (Svensson et al., 2008). For our purpose, we scale the δ^{18}O records to thermal histories and assume a constant temperature prior to 60 ka (Fig. 7a). For each thermal history, the present day trapped charge concentrations ($\bar{n}_{obs}$) are calculated for four TL thermometer (210-250 °C, 10 °C interval). The results reported in Fig. 7b-d show a clear depletion of the trapped charge population during the last 20 kyr, for all investigated scenarios. However, high frequency temperature variations are dampened, implying that TL thermometry is insensitive to short term variations. This result is consistent with the results shown in Fig. 4. For the inverse modelling, we first generate a large number of random periodic histories (300,000) assuming that they all follow the Greenland ice core δ^{18}O record (Svensson et al., 2008), which we scaled randomly by varying the amplitude of the temperature oscillation (i.e., the difference between minimum the temperature, which is at ~20 ka, and the maximum temperature at present) between 0 and 40 °C and the minimum temperature (i.e., temperature at ~20 ka) from -20 to 30 °C (see supplement S2). Note that making this assumption is somewhat equivalent to assuming a prior estimated on the inferred thermal history (Tarantola, 2005). The inversion results for three tested thermal histories are shown in Fig. 7e-p. The probability density functions (Fig. 7e, f and g) show it is possible to recover all three thermal histories within the 1σ confidence level using this inversion approach.

Figure 7

Deleted: .,

Moved (insertion) [3]

Formatted: Font color: Text 1

Formatted: Font color: Text 1

Formatted: Font color: Text 1

Formatted: Font color: Text 1

Moved (insertion) [6]

Formatted: Font color: Text 1

Moved (insertion) [2]

Moved (insertion) [4]

Moved (insertion) [5]

Moved (insertion) [7]

Moved (insertion) [8]

Deleted: The inversion results for three tested thermal histories are shown in Fig. 7. The probability density functions (Fig. 7a, b and c

4 Proof of concept

The following sections explore the potential of multi TL thermometers in the lower temperature region of the TL glow curve (210-250 °C) to infer the rock temperature histories for two samples collected in the European Alps.

4.1 Sample location

Two bedrock samples (MBTP1 and MBTP9) were collected at the Mer de Glace glacier (Mont Blanc massif, European Alps) at an altitude of 2545 and 2133 m. The rock surfaces were exposed since the last glacial maximum (LGM); with exposure ages younger than the LGM of about 20 kyr, based on ^{10}Be terrestrial cosmogenic nuclide and OSL surface exposure dating (Lehmann et al., 2019; Lehmann et al., 2020).

Deleted: 2019a

Deleted: 2019b

4.2 Sample preparation

The sample preparation followed the method reported previously (King et al., 2016b). The light exposed outer layer (>2 cm from the surface) was removed using a diamond saw under subdued red-light conditions with constant water flow to avoid frictional heating. The interior part of the sample was gently crushed with a mortar and pestle and sieved to separate the 150–250 µm grain size. The samples were sequentially treated with 10% HCl and 30% H_2O_2 to remove carbonate and organic matter respectively. Once dried, the magnetic fractions were removed using a hand magnet. The K-feldspar fraction was separated by density separation (<2.58 gm/cm^3) using sodium polytungstate. The grains were mounted on stainless steel discs using Silko-spay. Small aliquots of 2 mm diameter (containing ~100 grains) were prepared as these feldspars were highly luminescent.

Deleted: of these samples

4.3 Experimental procedure

The TL luminescence measurements were made using a Risø TL/OSL reader (TL/OSL DA- 20; Bøtter-Jensen et al., 2010) equipped with a ^{90}Sr/^{90}Y irradiation source (~ 0.24 Gy/s) at the University of Lausanne. A heating rate of 1 °C/s was used, under constant flow of N_2 gas. The TL emission was restricted to violet-blue (395±30 nm) using a filter combination of BG3 and BG39. The measurement details are discussed below. Typically, the minimum detectable limit for the present instrument is ~ 300 photon counts per second (cps) considering the signal should be three times of background level which is ~ 100 cps. The present high luminescent feldspar has maximum photon count of ~10^6 cps. This restricts to use the TL signals up to ~10^{-3} % of maximum TL signals.

Deleted: restrict

4.3.1 Measurements

Following Biswas et al. (2018), three sets of experiments were performed to constrain the growth parameters (D_0, a), thermal decay parameters (E, s, b) and athermal decay parameters (ρ'). The athermal frequency factor ($\bar{s}$) is taken as 3 ×10^{15} s^{-1} (Huntley, 2006).

The growth parameters and the natural TL level, i.e., the trapped charge population ($\bar{n}_{obs}$), are estimated using the multiple aliquot regeneration dose (MAR) protocol (Aitken, 1985) with post-glow normalization (Tang and Li, 2017). Eight regeneration doses (0, 24, 47, 118, 236, 472, 944 and 1888 Gy) were given and three aliquots were used for each dose point. A cut-heat of 200 °C was applied to remove traps that are unstable over laboratory timescales. We observed a significant sensitivity change (decrease) during the very first measurement of natural TL, which means that natural and regenerative TL signals were not measured under identical TL sensitivity conditions. To circumvent this sensitivity change, we adopted the

natural correction factor method (NCF; Chauhan and Singhvi, 2019; Singhvi et al., 2010; Singhvi et al., 2011). However, the NCF was initially developed for quartz OSL (Singhvi et al., 2011), it should to be adapted for feldspar.

The NCF method for quartz relies on the fact that the 110 °C TL peak and the blue stimulated OSL are correlated (Singhvi et al., 2011). In contrast, TL of feldspar does not exhibit a distinct 110 °C TL peak. The luminescence process in feldspar is more complicated because it arises from a continuous distribution of trapping energies and the dose response characteristics (D_0) varies along TL glow curve (Fig. 1). To circumvent these issues, we proceeded as follows. We first give a small dose (i.e., <100 Gy) in addition to the natural dose and subsequently measure the TL signal up to 200 °C (TL_1). Then the sample is annealed by heating it to 450 °C, which is followed by a dose of the same amount and measurement of the TL glow curve to 200 °C (TL_2). We observe that the TL sensitivity of the natural measurement is higher than the post natural regeneration measurement (Fig. 8a). We then calculate the NCF at different temperature between 90 to 150 °C, similar to the use of the 110 °C TL peak for quartz. We find that the NCF decreases with increasing temperature during the TL measurement (Fig. 8c). Since there is no direct way to measure the NCF beyond 150 °C, we then extrapolate the NCF value at the region of interest to higher temperatures, i.e., 210-250 °C (Fig. 8c), which we call var-NCF. In turn, the trapped charge population ($\bar{n}_{obs}$) is corrected with the corresponding factor which is in between 1 and 2 for sample MBTP1 and MBTP9 (Table 1 and Fig. 8). Finally, we investigated the effects of variable doses and the NCF and found it had no effect for doses below 100 Gy (Fig. 8b).

Figure 8

The thermal decay parameters are estimated using the T_m–T_{stop} method (McKeever, 1980) and analyzed by subtraction and fitting of sub-peaks (Pagonis et al., 2014). For the athermal decay parameter, a fading experiment (Huntley and Lian, 2006) was performed for different delay times; aliquots were preheated to 200 °C prior to storage.

4.3.2 Estimating the kinetic parameters

The kinetic parameters of growth (D_0, a), thermal decay (E, s, b) and athermal decay (ρ') were inferred using the approach of Biswas et al. (2018) for all thermometers (210-250 °C, 10 °C interval). The results are summarized in Table 1 and shown in supplementary material S3. The dose rate ($\dot{D}$) values, another growth parameter, were taken from Lehmann et al. (2020). Since a cut-heat of 200 °C was applied for the MAR growth analysis and fading experiments, we focus on the 210-250 °C TL thermometers (i.e., four thermometers). We did not use TL signals beyond 250 °C, as they are insensitive to typical surface temperature fluctuations, as discussed in section 2.2.

Table 1

4.4 Predicting the surface temperature

The measured TL signals ($\bar{n}_{obs}$) are then inverted to infer the thermal history as described in section 3.2 and 3.4 (Synthetic approach 2). For the thermal histories, we again use the Greenland ice core $\delta^{18}O$ record (Svensson et al., 2008), which we scaled as described in section 3.2. We assume that the atmospheric temperatures of the Mont Blanc massif followed the trend observed for the Greenland ice core data over the last 60 ka. Note that temperature increase during the last glacial cycle was synchronous with the temperature anomalies observed in Greenland (e.g., Heiri et al., 2014; Schwander et al., 2000; van Raden et al. 2013). The rationale here is that all temperatures in the Mont Blanc massif follow the Greenland ice core $\delta^{18}O$ data but the amplitude of temperature oscillation (minimum temperature at ~20 ka to maximum temperature at the present day) and mean temperature are unknown. We pick the amplitude of temperature oscillation randomly between 0 and 40 °C, and the base temperature (temperature at ~20 ka) between -20 and 30 °C. By generating a large number of random thermal histories

Deleted: and

Deleted: .

Deleted: anomalies

Deleted: It is assumed

Deleted: since

Deleted: kyr

Formatted: Font color: Auto

(300,000), the probability density function is constructed as discussed in section 3.2. The results of two samples, MBTP1 and MBTP2, are shown in Fig. 9 and suggest that the temperature rose from $-4.6^{+3.7}_{-4.1}$ to $6.2^{+3.1}_{-3.5}$ °C for sample MBTP1 and $-2.0^{+3.9}_{-4.1}$ to $7.9^{+3.0}_{-3.1}$ °C for sample MBTP9, since 20 ka, considering one sigma uncertainty. The inferred median suggests an increase of ~10-11 °C for the rock surface temperature over the last 20 ka.

Figure 9

5 Discussion

The theoretical model for the rate equation of trapped charge population in feldspar has been described in several ways; first order kinetics (Brown and Rhodes, 2017; Yukihara et al., 2018), general order kinetics (Biswas et al., 2018; Guralnik et al., 2015b), charge transport through sub-conduction band-tail states (King et al., 2016a; Li and Li, 2013), Gausian distribution of trapped energies (Lambert et al., In Revision), or localized recombination in randomly distributed defects (Jain et al., 2012). What is common to all these models is that luminescence of feldspar is complicated and exhibit a non-linear non-first order kind of behaviour due to either presence of sub-conduction band-tail states (Morthekai et al., 2019; Poolton et al., 2002) or complex charge transport mechanism. TL in feldspar is even more complicated because it shows continuous distribution of trapping energies (Biswas et al., 2018; Duller, 1997; Grün and Packman, 1994; Pagonis et al., 2014; Strickertsson, 1985) and TL is a more diffusive process than OSL; OSL of feldspar has resonant energy levels (Hütt et al., 1988). Different models were reviewed and tested by Guralnik et al. (2015b) who suggested that the general order kinetic, a mathematically simplified model, could be used to explain luminescence phenomenon well. We adopted this model for TL of feldspar where the power terms (a, b) accounts for the nonlinearity involved in the TL of feldspar. The efficacy of using general order kinetics has been demonstrated to samples with known thermal history (KTB borehole samples) for OSL of feldspar (Guralnik et al., 2015a) and TL of feldspar (Biswas et al., 2018).

Here we investigate the difference in temperature sensitivity of different TL thermometers, which correspond to individual TL temperature or TL signals. On the basis of the kinetic parameters derived for our sample, and our sensitivity tests (section 2.2.1), we recommend using TL thermometers with temperature range of 200 to 250 °C for a typical surface temperature fluctuation, e.g. ~10 °C. If the temperature fluctuations are larger, higher temperature TL (>250 °C TL) can be used. The multiple TL signal (200 to 250 °C, 10 °C interval) can constrain thermal history of ~50 kyr. A higher temperature fluctuation can be better constrained with a greater number of thermometers (as discussed in section 2.2.1).

For periodic oscillations, when the period is comparable to the lifetime of the trapped electron for a given thermometer, it may be used to infer temporal variation of surface temperature (see section 2.2.2). Typically, tens of kyr of temperature oscillation can be detected using TL thermometers with peak temperatures higher than 200 °C (210 to 250 °C). Periodic oscillation with lower period (<1 kyr) will exhibit a similar effect to isothermal temperature condition, yielding a temperature higher than the mean of oscillation.

One outstanding issue when using TL is the sensitivity change during the very first measurements up to 450 °C, which cannot be corrected by post-glow normalization (Tang and Li, 2017). Here we show that sensitivity changes during natural measurements can be monitored for lower temperature TL (<150 °C) following the same method adopted for the OSL of quartz, which is called the natural correction factor (NCF; Singhvi et al., 2011). Because there is no direct method to track the TL sensitivity change in the region of interest (210-250 °C TL), we simply extrapolate the sensitivity change observed in the lower temperature TL peaks (i.e., 90-150 °C) to the region of interest (i.e., 210-250 °C). This is new and it will need further investigation. However, we find that the effect of the initial sensitivity change on the amplitude of the inferred temperature

Deleted: 10

Deleted: kyr

histories is small. In Fig. 10, we compare inversion results for three different scenarios for sample MBTP1; 1) there is no initial sensitivity correction, i.e., NCF =1; 2) the initial sensitivity correction is done using the value obtained at 100 °C (NCF_{100}=1.64±0.08); and 3) the var-NCF approach described in the section 4.3.1 is used. Although the results show that the sensitivity correction has a significant impact on the absolute inferred temperature, we do not observe much difference between using a constant value and the extrapolated value. Furthermore, and more importantly, the difference between the present-day temperature and temperature about 20 ka remains about 10-11°C in the three tested cases (median of the prediction).

Figure 10

The estimated constant erosion rates in these two sample locations, MBTP1 and MBTP9, are 3.5×10^{-3} and 3.2×10^{-2} mm/yr with maximum possible time of erosion of 20.9 and 19.5 ka respectively (Lehman et al. 2020). This translates to a maximum erosion depth in these two locations are 0.07 and 0.62 m respectively. At those depths, mean temperature should be in equilibrium with atmospheric temperature (e.g., Hasler et al. 2011). Based on the rock temperature measurement of borehole samples in Mont-Blanc massif, Magnin et al. (2017) suggest up to a 2 m depth the rock temperature is constant with depth.

For the inverse modeling of natural samples, $\delta^{18}O$ data are used as a prior on the shape of the thermal histories, but we leave two scaling parameters free – minimum temperature at 20 ka, and amplitude (temperature difference between at 20 ka and present)– and we did not include the role of ice on setting the rock temperature during glaciation. Lehman et al. (2020) provided a range of solution for deglaciation in the present location, either thinning of 450 m glacier occurred progressively between ~17 ka and ~12 ka or it was instantaneous. In absence of clear scenario, we took two samples from two extreme altitudes of 2545 (MBTP1) and 2133 (MBTP9). The top most sample, MBTP1, had a very thin or no glacier covered during LGM, and the bottom most sample, MBTP9, was exposed or covered by ice. Thus, it is expected that the during LGM, rock temperature of MBTP1 would have been in equilibrium with atmospheric temperature (Hoelzle et al. 1999) whereas it is less clear for MBTP9. If it was covered by ice, it was likely temperate ice and the basal temperature would be close to 0 °C. Interestingly, we find similar results from the inversion; predicted rock surface temperatures of MBTP1 and MBTP9, during LGM, are $-4.6^{+3.7}_{-4.1}$ and $-2.0^{+3.9}_{-4.1}$ respectively; temperature of the bottom most sample during LGM is close to 0 °C, at least within error.

The application of the introduced method predicts that the final rock surface temperatures at the locations of Mont-Blanc massif are 6.2 ± 3.2 °C for MBTP1 (2545 m) and 7.9 ± 3.0 °C for sample MBTP9 (2133). Although these temperatures have large uncertainty, they are higher than the mean annual atmospheric temperature in this location. The mean annual temperature of Chamonix (1035 m), a nearby city, is 7.3 °C. Considering an adiabatic lapse rate of 5 °C/km, the expected mean annual atmospheric temperatures at the sample location of MBTP1 and MBTP9 are ~0 and 2 °C respectively. The offset between the predicted and expected temperature (~6 °C) can be explained by two main reasons: 1) the rock surface temperature is always higher than atmospheric temperature and the temperature difference can be up to 10 °C (Magnin et al., 2019), and 2) seasonal temperature fluctuations may lead to an overestimation of the mean annual temperature (as discussed in section 2.2.2). To quantify this latter offset, we performed a simple synthetic test, with annual oscillation of +10 °C (summer) to -10°C (winter) with mean at 0 °C, up to 20 ka (before that temperature was set to a 0 °C isotherm), and predicted the equivalent isothermal temperature using the inverse approach. The result suggests a mean annual temperature that is 2.7±0.7 °C higher than the mean temperature of the periodic signal (Fig. 11), confirming the results of Guralnik and Sohbati (2019).

Figure 11

The inverse modeling results show an increase of rock surface temperature in the Mont Blanc Massif of ~10-11 °C (considering median of the prediction) from 20 ka to today. The median of the distribution of possible thermal histories of the two samples follows Greenland ice core $\delta^{18}O$ anomalies with missing of low frequencies. Climate reconstructions in Europe using fossil

Deleted: kyr

Deleted: 2019b

Deleted: depths

Deleted: constant (e.g.

Deleted: (Magnin pers. comm).

Deleted: sample, the time-

Deleted: histories were completely random

Deleted: put any constrain for

Deleted: cover artefact

Deleted: LGM

Deleted: 2019b

Deleted: after

Deleted: had thick glacier.

Deleted: , high over burden pressure

Deleted: melting condition would fix

Deleted: We

Deleted: the

Deleted: of inferences

Deleted: inferred

Deleted: history

pollen suggest that the mean annual temperature anomaly (the difference between the temperature at the LGM and today) is 12±3 °C in the north of Pyrenees–Alps line (Peyron et al., 1998). Wu et al. (2007) inferred that LGM temperatures in Europe were ~ 10-15 °C lower than the present-day temperature based on pollen analysis. Although there are large uncertainties associated with pollen data and having its methodological constrain, the overlap in temperature estimates between the two proxies suggest that TL may be a reliable paleothermometer.

6 Conclusions

A new approach to reconstruct the temporal variation of rock surface temperature using the TL of feldspar is introduced. Forward modeling of different TL signals suggests that TL signals in the range of 210 to 250 °C are sensitive to typical surface temperature fluctuations, which we define as TL thermometers. Multiple TL thermometers (210-250 °C, 10 °C interval) can then be used to constrain thermal histories of rocks over ~50 kyr for temperature fluctuations of ~10 °C. The sensitivity of the periodic forcing on trapped charge populations suggest that natural TL is sensitive enough to mean temperature and amplitude of periodic forcings. Typically, tens of kyr of temperature oscillation can be predicted using this approach. Finally, we show that it is possible to recover thermal histories of rocks when one assumes that the temperature followed observed Greenland ice core $\delta^{18}O$ record.

Deleted: anomalies. Based on analysis of two samples from Mont Blanc Massif, European Alps, it can be suggested that the LGM was ~ 10-11 °C colder than the present day.

Code/data availability

The raw data files and Matlab codes can be obtained by requirement to the corresponding author.

Author contribution

RHB and FH conceived the idea. RHB, FH and GEK conceptualized the study. RHB designed the experiments and numerical modelling with inputs from FH. BL collected the samples and looked into the Geological aspects of the location. Sample preparation, measurement and analysis were made by RHB with inputs from AKS. RHB wrote the paper with input from all co-authors.

Competing interests

The authors declare that they have no conflict of interest.

Acknowledgements

RHB acknowledge University of Lausanne for support and Prof. Jean Braun for insightful discussions. We thank Benny Guralnik for his astute opinion on this work. Florence Magnin is thanked to help us understand the present rock temperature scenarios. AKS thanks the Indian Department of Science and Technology, SERB- Year of Science Chair Professorship.

Deleted: discussion

References

Aitken, M.J.: Thermoluminescence dating. Academic press, London, 1985.

Bartlein, P.J., Harrison, S.P., Brewer, S., Connor, S., Davis, B.A.S., Gajewski, K., Guiot, J., Harrison-Prentice, T.I., Henderson, A., Peyron, O., Prentice, I.C., Scholze, M., Seppä, H., Shuman, B., Sugita, S., Thompson, R.S., Viau, A.E., Williams, J., Wu, H.: Pollen-based continental climate reconstructions at 6 and 21 ka: a global synthesis, Climate Dynamics, 37, 775-802, 2011.

Biswas, R.H., Herman, F., King, G.E., Braun, J.: Thermoluminescence of feldspar as a multi-thermochronometer to constrain the temporal variation of rock exhumation in the recent past, Earth and Planetary Science Letters, 495, 56-68, 2018.

Bøtter-Jensen, L., Thomsen, K.J., Jain, M.: Review of optically stimulated luminescence (OSL) instrumental developments for retrospective dosimetry, Radiation Measurements, 45, 253-257, 2010.

Braun, J., van der Beek, P., Valla, P., Robert, X., Herman, F., Glotzbach, C., Pedersen, V., Perry, C., Simon-Labric, T., Prigent, C.: Quantifying rates of landscape evolution and tectonic processes by thermochronology and numerical modeling of crustal heat transport using PECUBE, Tectonophysics, 524-525, 1-28, 2012.

Brown, N.D., Rhodes, E.J., Harrison, T.M.: Using thermoluminescence signals from feldspars for low-temperature thermochronology, Quaternary Geochronology, 42, 31-41, 2017.

Chauhan, N., Singhvi, A.K.: Changes in the optically stimulated luminescence (OSL) sensitivity of single grains of quartz during the measurement of natural OSL: Implications for the reliability of optical ages, Quaternary Geochronology, 53, 101004, 2019.

Duller, G.A.T.: Behavioural studies of stimulated luminescence from feldspars, Radiation Measurements, 27, 663-694, 1997.

Durrani, S.A., Khazal, K.A.R., Ali, A.: Temperature and duration of the shadow of a recently-arrived lunar boulder, Nature, 266, 411-415, 1977.

Gallagher, K., Charvin, K., Nielsen, S., Sambridge, M., Stephenson, J.: Markov chain Monte Carlo (MCMC) sampling methods to determine optimal models, model resolution and model choice for Earth Science problems, Marine and Petroleum Geology, 26, 525-535, 2009.

Grün, R., Packman, S.C.: Observations on the kinetics involved in the TL glow curves in quartz, K-feldspar and Na-feldspar mineral separates of sediments and their significance for dating studies, Radiation Measurements, 23, 317-322, 1994.

Guralnik, B., Jain, M., Herman, F., Ankjærgaard, C., Murray, A.S., Valla, P.G., Preusser, F., King, G.E., Chen, R., Lowick, S.E., Kook, M., Rhodes, E.J.: OSL-thermochronometry of feldspar from the KTB borehole, Germany, Earth and Planetary Science Letters, 423, 232-243, 2015a.

Guralnik, B., Li, B., Jain, M., Chen, R., Paris, R.B., Murray, A.S., Li, S.-H., Pagonis, V., Valla, P.G., Herman, F.: Radiation-induced growth and isothermal decay of infrared-stimulated luminescence from feldspar, Radiation Measurements, 81, 224-231, 2015b.

Guralnik, B., Sohbati, R., 2019. Fundamentals of Luminescence Photo-and Thermochronometry, Advances In Physics And Applications Of Optically And Thermally Stimulated World Scientific, p. 475.

Hasler, A., Gruber, S., Haeberli, W.: Temperature variability and offset in steep alpine rock and ice faces, The Cryosphere, 5, 977-988, 2011.

Heiri, O., Koinig, K.A., Spötl, C., Barrett, S., Brauer, A., Drescher-Schneider, R., Gaar, D., Ivy-Ochs, S., Kerschner, H., Luetscher, M., Moran, A., Nicolussi, K., Preusser, F., Schmidt, R., Schoeneich, P., Schwörer, C., Sprafke, T., Terhorst, B., Tinner, W.: Palaeoclimate records 60–8 ka in the Austrian and Swiss Alps and their forelands, Quaternary Science Reviews, 106, 186-205, 2014.

Deleted: 2015

Herman, F., King, G.E.: Luminescence Thermochronometry: Investigating the Link between Mountain Erosion, Tectonics and Climate, Elements, 14, 33-38, 2018.

Herman, F., Rhodes, E.J., Braun, J., Heiniger, L.: Uniform erosion rates and relief amplitude during glacial cycles in the Southern Alps of New Zealand, as revealed from OSL-thermochronology, Earth and Planetary Science Letters, 297, 183-189, 2010.

Hoelzle, M., Wegmann, M., Krummenacher, B.: Miniature temperature dataloggers for mapping and monitoring of permafrost in high mountain areas: first experience from the Swiss Alps, Permafrost and Periglacial Processes, 10, 113-124, 1999.

Huntley, D.J.: An explanation of the power-law decay of luminescence, Journal of Physics: Condensed Matter, 18, 1359-1365, 2006.

Huntley, D.J., Lian, O.B.: Some observations on tunnelling of trapped electrons in feldspars and their implications for optical dating, Quaternary Science Reviews, 25, 2503-2512, 2006.

Jain, M., Guralnik, B., Andersen, M.T.: Stimulated luminescence emission from localized recombination in randomly distributed defects, Journal of Physics: Condensed Matter, 24, 385402, 2012.

Jones, P.D., Mann, M.E.: Climate over past millennia, Reviews of Geophysics, 42, 2004.

Kars, R.H., Wallinga, J., Cohen, K.M.: A new approach towards anomalous fading correction for feldspar IRSL dating — tests on samples in field saturation, Radiation Measurements, 43, 786-790, 2008.

King, G.E., Herman, F., Guralnik, B.: Northward migration of the eastern Himalayan syntaxis revealed by OSL thermochronometry, Science, 353, 800-804, 2016a.

King, G.E., Herman, F., Lambert, R., Valla, P.G., Guralnik, B.: Multi-OSL-thermochronometry of feldspar, Quaternary Geochronology, 33, 76-87, 2016b.

King, G.E., Tsukamoto, S., Herman, F., Biswas, R.H., Sueoka, S., Tagami, T.: ESR-thermochronometry of the Hida range of the Japanese Alps: Validation and future potential, Geochronology Discuss., 2019, 1-24, 2019.

Lambert, R., King, G.E., Valla, P.G., Herman, F.: Validating multiple first-order kinetic models for feldspar thermal decay in luminescence thermochronometry. Radiation Measurements, *In Revision.*

Lehmann, B., Herman, F., Valla, P.G., King, G.E., Biswas, R.H.: Evaluating post-glacial bedrock erosion and surface exposure duration by coupling in situ optically stimulated luminescence and 10Be dating, Earth Surf. Dynam., 7, 633-662, 2019.

Lehmann, B., Herman, F., Valla, P.G., King, G.E., Biswas, R.H., Ivy-Ochs, S., Kroning, O., Christl, M.: Post-glacial erosion of polished bedrock surfaces and deglaciation timing: new insights from the Mont Blanc massif (Western Alps), Geology, 48, 139-144, 2020.

Li, B., Li, S.-H.: Determining the cooling age using luminescence-thermochronology, Tectonophysics, 580, 242-248, 2012.

Li, B., Li, S.-H.: The effect of band-tail states on the thermal stability of the infrared stimulated luminescence from K-feldspar, Journal of Luminescence, 136, 5-10, 2013.

Magnin, F., Josnin, J.Y., Ravanel, L., Pergaud, J., Pohl, B., Deline, P.: Modelling rock wall permafrost degradation in the Mont Blanc massif from the LIA to the end of the 21st century, The Cryosphere, 11, 1813-1834, 2017.

Magnin, F., Etzelmüller, B., Westermann, S., Isaksen, K., Hilger, P., Hermanns, R.L.: Permafrost distribution in steep rock slopes in Norway: measurements, statistical modelling and implications for geomorphological processes, Earth Surf. Dynam., 7, 1019-1040, 2019.

Deleted: 2019a

Deleted: 2019b

McKeever, S.W.S.: On the analysis of complex thermoluminescence. Glow-curves: Resolution into individual peaks, physica status solidi (a), 62, 331-340, 1980.

Morthekai, P., Biswas, R.H., Singhvi, A.K.: Charge transport in band-tail states of irradiated alkali feldspar I: Super-Arrhenius kinetics, Physica B: Condensed Matter, 561, 103-110, 2019.

Pagonis, V., Morthekai, P., Kitis, G.: Kinetic analysis of thermoluminescence glow curves in feldspar: evidence for a continuous distribution of energies, Geochronometria, 41, 168-177, 2014.

Peyron, O., Guiot, J., Cheddadi, R., Tarasov, P., Reille, M., de Beaulieu, J.-L., Bottema, S., Andrieu, V.: Climatic Reconstruction in Europe for 18,000 YR B.P. from Pollen Data, Quaternary Research, 49, 183-196, 1998.

Poolton, N.R.J., Ozanyan, K.B., Wallinga, J., Murray, A.S., Bøtter-Jensen, L.: Electrons in feldspar II: a consideration of the influence of conduction band-tail states on luminescence processes, Physics and Chemistry of Minerals, 29, 217-225, 2002.

Ronca, L.B.: Minimum length of time of frigid conditions in Antarctica as determined by thermoluminescence, American Journal of Science, 262, 767-781, 1964.

Ronca, L.B., Zeller, E.J.: Thermoluminescence as a function of climate and temperature, American Journal of Science, 263, 416-428, 1965.

Schwander, J., Eicher, U., Ammann, B.: Oxygen isotopes of lake marl at Gerzensee and Leysin (Switzerland), covering the Younger Dryas and two minor oscillations, and their correlation to the GRIP ice core, Palaeogeography, Palaeoclimatology, Palaeoecology, 159, 203-214, 2000.

Singhvi, A.K., Chauhan, N., Biswas, R.H.: A Survey Of Some New Approaches In Extending The Maximum Age Limit And Accuracy Of Luminescence Application To Archaeological Chronometry, Mediterranean Archaeology and Archaeometry, 10, 9-15, 2010.

Singhvi, A.K., Stokes, S.C., Chauhan, N., Nagar, Y.C., Jaiswal, M.K.: Changes in natural OSL sensitivity during single aliquot regeneration procedure and their implications for equivalent dose determination, Geochronometria, 38, 231-241, 2011.

Strickertsson, K.: The thermoluminescence of potassium feldspars—Glow curve characteristics and initial rise measurements, Nuclear Tracks and Radiation Measurements (1982), 10, 613-617, 1985.

Svensson, A., Andersen, K.K., Bigler, M., Clausen, H.B., Dahl-Jensen, D., Davies, S.M., Johnsen, S.J., Muscheler, R., Parrenin, F., Rasmussen, S.O., Röthlisberger, R., Seierstad, I., Steffensen, J.P., Vinther, B.M.: A 60 000 year Greenland stratigraphic ice core chronology, Clim. Past, 4, 47-57, 2008.

Tachiya, M., Mozumder, A.: Decay of trapped electrons by tunnelling to scavenger molecules in low-temperature glasses, Chemical Physics Letters, 28, 87-89, 1974.

Tang, S.-L., Li, S.-H.: Low temperature thermochronology using thermoluminescence signals from K-feldspar, 44, 112, 2017.

Tarantola, A.: Inverse Problem Theory and Methods for Model Parameter Estimation. Siam, 2005.

Tierney, J.E., Schouten, S., Pitcher, A., Hopmans, E.C., Sinninghe Damsté, J.S.: Core and intact polar glycerol dialkyl glycerol tetraethers (GDGTs) in Sand Pond, Warwick, Rhode Island (USA): Insights into the origin of lacustrine GDGTs, Geochimica et Cosmochimica Acta, 77, 561-581, 2012.

Tremblay, M.M., Shuster, D.L., Balco, G.: Cosmogenic noble gas paleothermometry, Earth and Planetary Science Letters, 400, 195-205, 2014a.

Tremblay, M.M., Shuster, D.L., Balco, G.: Diffusion kinetics of 3He and 21Ne in quartz and implications for cosmogenic noble gas paleothermometry, Geochimica et Cosmochimica Acta, 142, 186-204, 2014b.

Wheelock, B., Constable, S., Key, K.: The advantages of logarithmically scaled data for electromagnetic inversion, Geophysical Journal International, 201, 1765-1780, 2015.

van Raden, U.J., Colombaroli, D., Gilli, A., Schwander, J., Bernasconi, S.M., van Leeuwen, J., Leuenberger, M., Eicher, U.: High-resolution late-glacial chronology for the Gerzensee lake record (Switzerland): δ18O correlation between a Gerzensee-stack and NGRIP, Palaeogeography, Palaeoclimatology, Palaeoecology, 391, 13-24, 2013.

Wintle, A.G.: Anomalous Fading of Thermo-luminescence in Mineral Samples, Nature, 245, 143-144, 1973.

Wu, H., Guiot, J., Brewer, S., Guo, Z.: Climatic changes in Eurasia and Africa at the last glacial maximum and mid-Holocene: reconstruction from pollen data using inverse vegetation modelling, Climate Dynamics, 29, 211-229, 2007.

Yukihara, E.G., Coleman, A.C., Biswas, R.H., Lambert, R., Herman, F., King, G.E.: Thermoluminescence analysis for particle temperature sensing and thermochronometry: Principles and fundamental challenges, Radiation Measurements, 120, 274-280, 2018.

Zachos, J., Pagani, M., Sloan, L., Thomas, E., Billups, K.: Trends, Rhythms, and Aberrations in Global Climate 65 Ma to Present, Science, 292, 686-693, 2001.

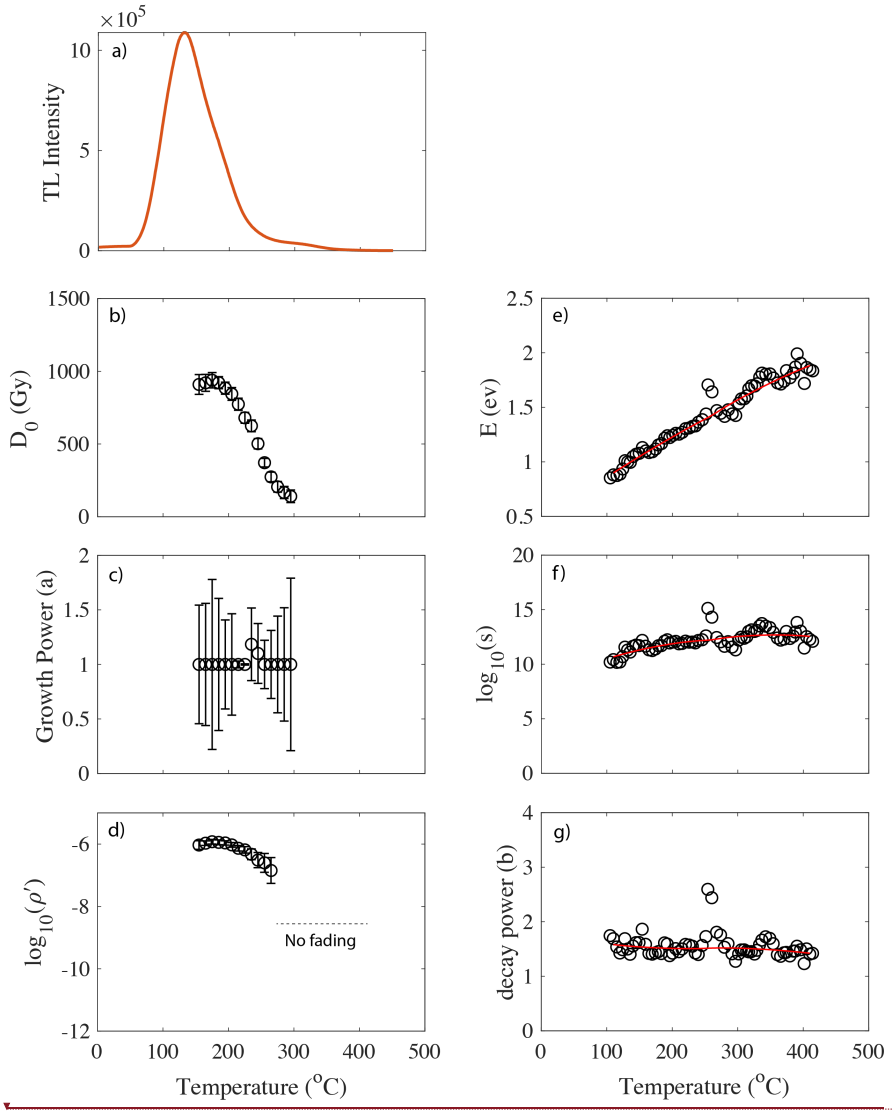

Deleted:

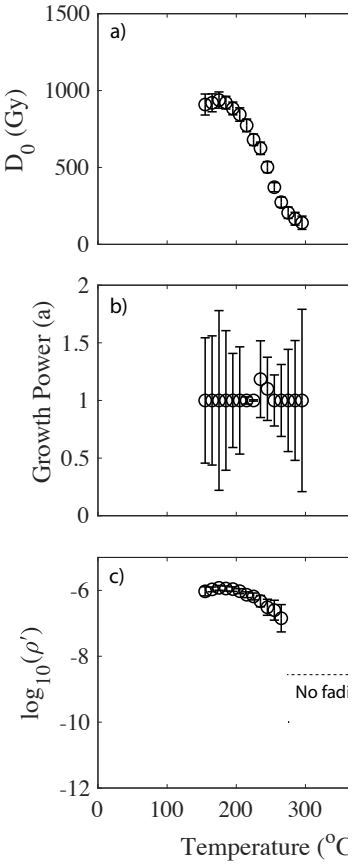

Figure 1: Inferred TL kinetic parameters from TL glow curve of sample MBTP9. The method used to constrain these parameters in the laboratory is fully explained in Biswas et al. (2018) and described in supplementary material S1.

Deleted: followed by

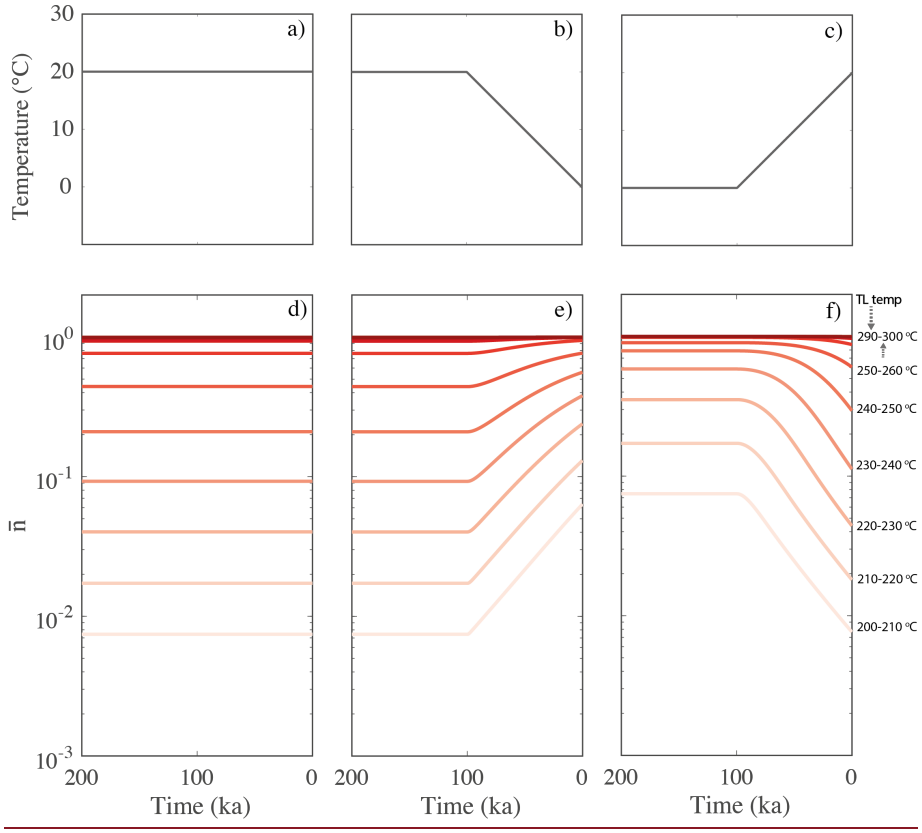

Figure 2: a, b, and c are the three prescribed thermal histories: isothermal, cooling and warming respectively. d, e and f are the corresponding dynamic equilibrium levels of trapped charge population ($\bar{n}$) of 10 different thermometers in the range of 200-300 °C. The temperature of the thermometers (or TL temperature) are shown on the right.

Deleted: in the right. The temperature of the corresponding thermometers (or TL temperature) are shown in the right.

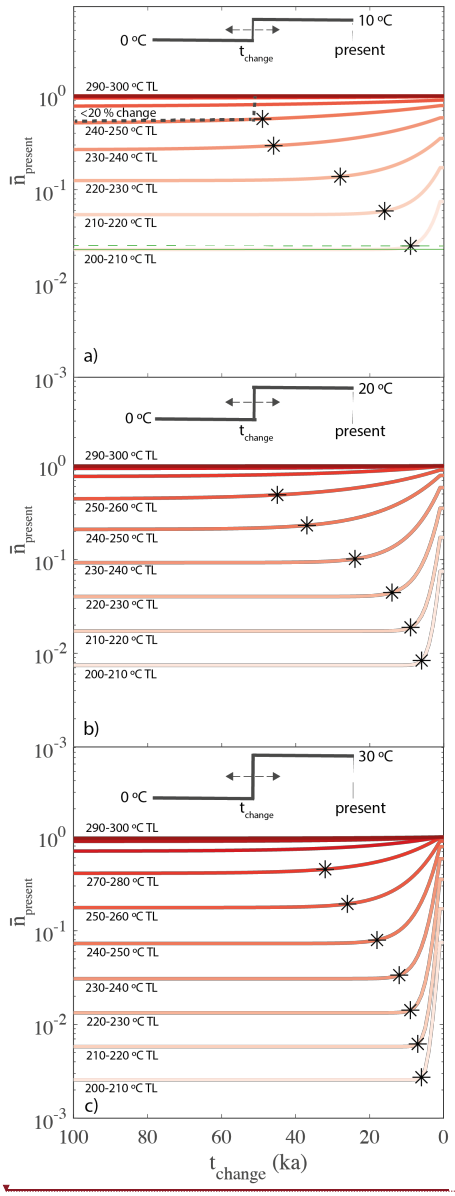

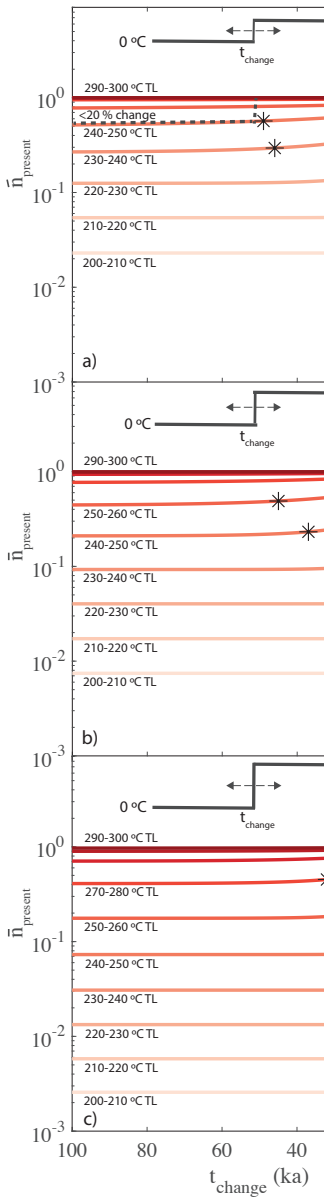

Figure 3: The variation of present day trapped charge population ($\bar{n}_{present}$) of different thermometers with time of change of temperature (t_{change}) of step function like thermal history with temperature change of a) 10 °C, b) 20 °C and c) 30 °C. The asterisk symbols denote the memory time (t_{memory}) that a thermometer can record the temperature change history. Estimation of t_{memory} is illustrated in plot a for 200-210 °C TL thermometer. The solid green line corresponds to $\bar{n}_{present}$ for t_{change}=100 ka, and the dashed green lines represent $\bar{n}_{present}$ for $t_{change} = t_{memory}$, which is 20% higher than the solid green line.

Deleted:

Deleted: height

Deleted: steps

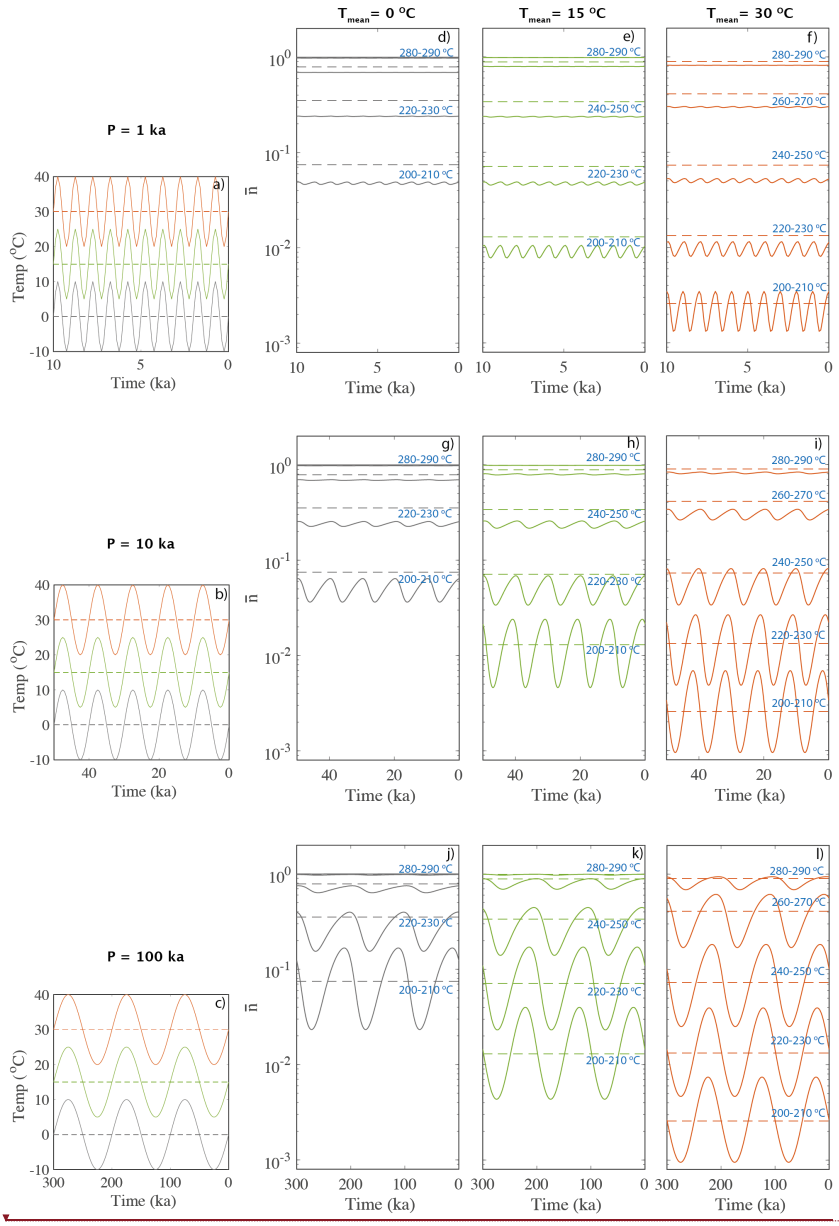

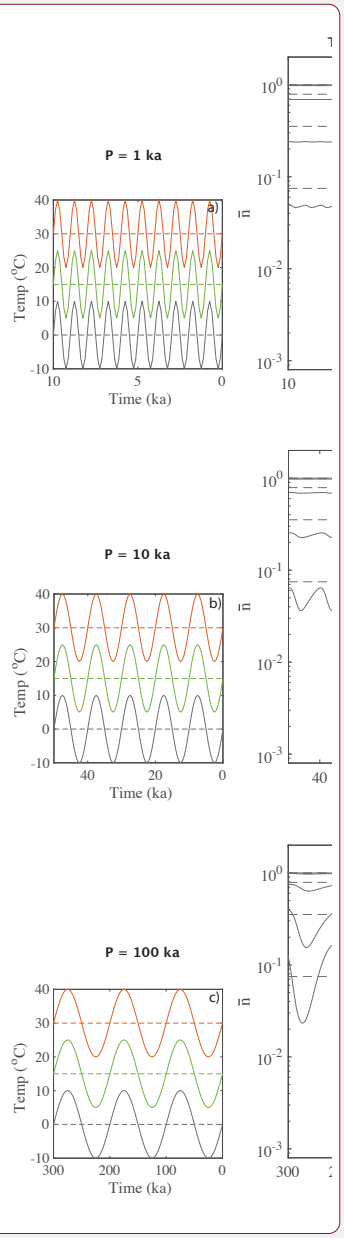

Deleted:

Figure 4: Variation of trapped charge population ($\bar{n}$) for different sinusoidal thermal histories. a, b, and c represents the prescribed thermal histories with same mean amplitude (10 °C) and three different mean temperatures (0, 15 and 30 °C) but for different periods, 1, 10 and 100 ka respectively. The dashed lines are the isotherm (mean temperature of oscillation). Fig. d-f, g-i, and j-l are the the response of $\bar{n}$ for the corresponding thermal field. The solid lines are for oscillating fields and dashed lines are for isothermal fields. The temperature of the representative thermometers (or TL temperature) are shown inside in blue.

Deleted: Fig.

Deleted: input

Deleted: periodicities

Deleted: corresponding

Deleted: the right

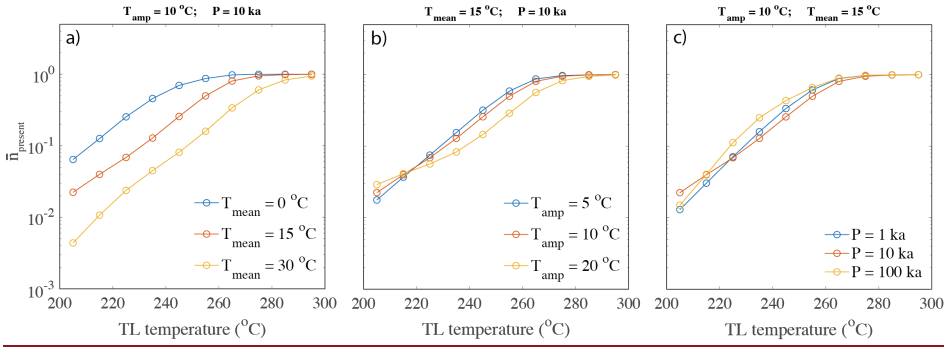

Figure 5: Present day trapped charge populations ($\bar{n}_{present}$) of different TL signals (or thermometers) with a) mean temperature variation (amplitude and period are fixed), b) amplitude variation (mean temperature and period are fixed), and c) period variation (mean temperature and amplitudes are fixed).

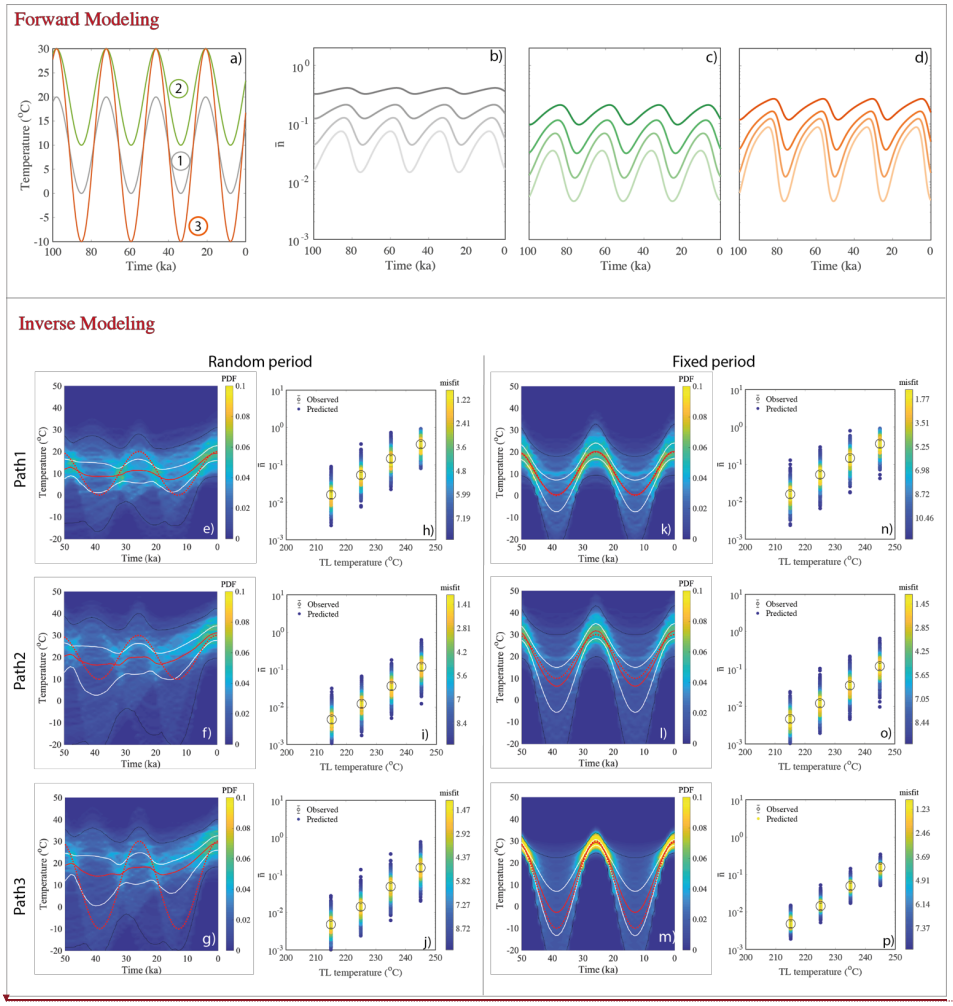

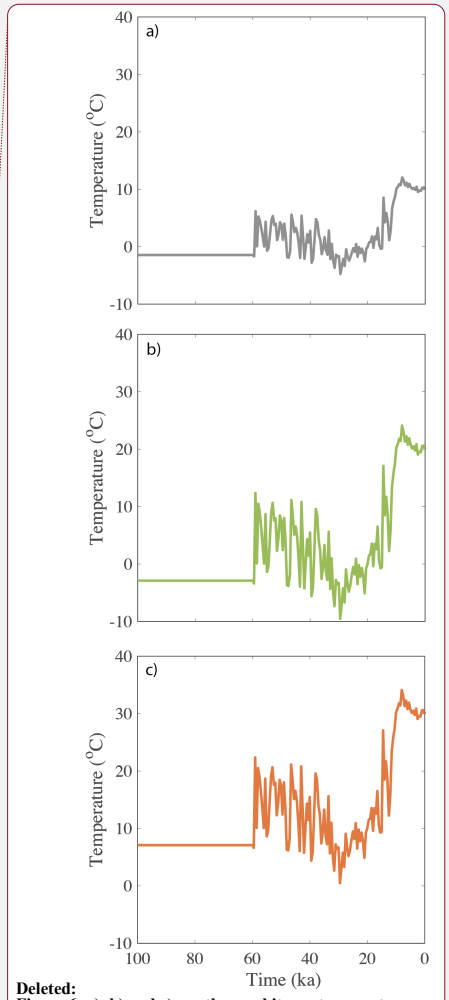

Deleted:
Figure 6: a), b) and c) are three arbitrary temperature histories obtained by scaling the Greenland $\delta^{18}O$ ice core anomalies

Figure 6: Results of synthetic experiment of approach 1, a-d) are for the forward modeling and e-p) are for the inverse modeling. a) three arbitrary periodic thermal histories with different mean temperature (T_{mean}) and amplitude (T_{amp}) but fixed period *P*. b), c) and d) are the evolution of trapped charge population ($\bar{n}$) for four different thermometers (210-250 °C, 10 °C interval) of the corresponding to three thermal histories, respectively. The present day trapped charge populations are considered as observed values ($\bar{n}_{obs}$) for the inverse modeling. e), f) and g) are the inferred probability density plots when T_{mean}, T_{amp} and *P* are randomly varied. h), i), and j) depict the fit between the observed TL (obtained through forward modeling). The solid red lines show the predicted median, white lines and black lines show the 1σ and 2 σ confidence intervals in the probability density distribution k), l) and m) are the inferred probability density functions when T_{mean}, and T_{amp} are randomly varied but *P* is fixed. n), o), and p) depict the fit between the observed TL (obtained through forward modeling). These results are obtained using the kinetic parameters of sample MBTP9.

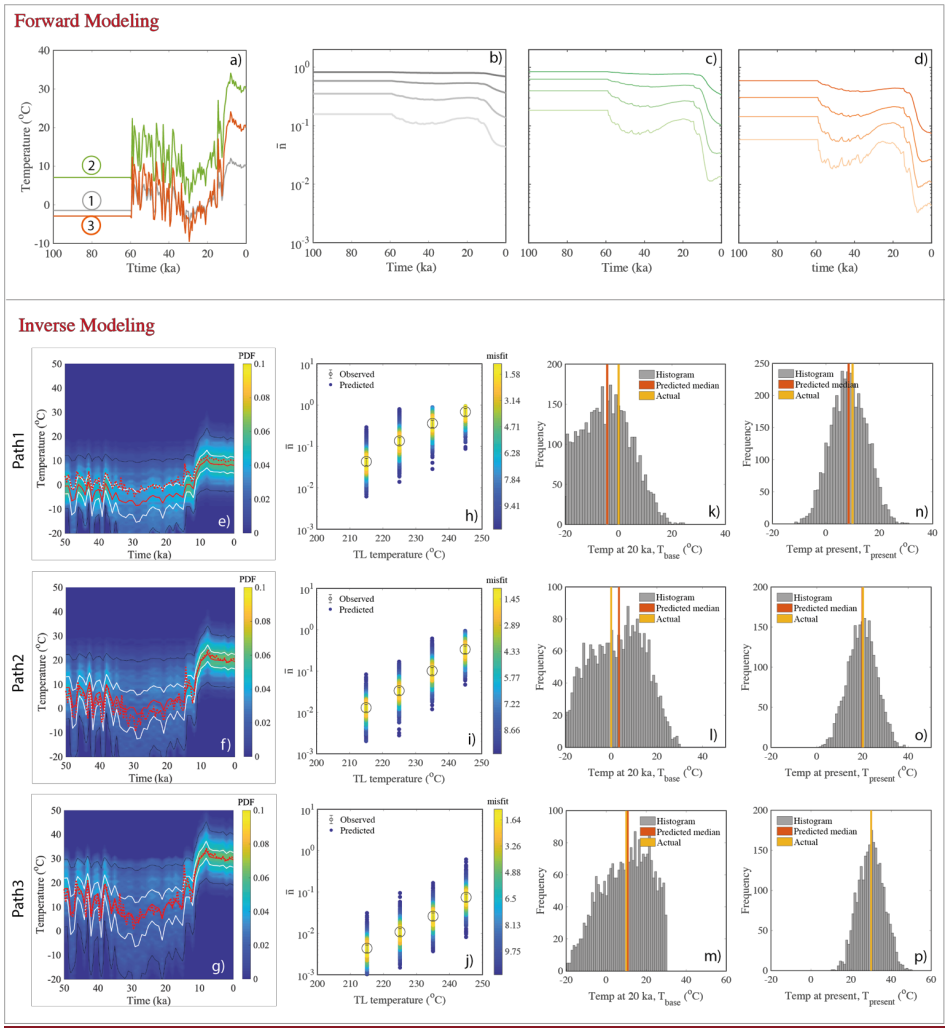

Figure 7: Results of synthetic experiment of approach 2, a-d) are for the forward modeling and e-p) are for the inverse modeling. a) three arbitrary temperature histories obtained by scaling the Greenland $\delta^{18}O$ ice core record (Svensson et al., 2008). b), c) and d) are the evolution of trapped charge population ($\bar{n}$) for four different thermometers (210-250 °C, 10 °C interval) corresponding to three histories respectively. The present day trapped charge populations are considered as observed value ($\bar{n}_{obs}$) for the inverse modeling. e), f) and g) are the inferred probability density functions. The dashed red lines show the actual temperature history as used in forward modeling, the solid red lines show the predicted median, white lines and black lines show the 1σ and 2σ confidence intervals in the probability density distribution. h), i), and j) depict the fit between the observed TL (obtained through forward modeling) and modelled TL (obtained through inverse modeling). k), l), and m) represent histograms of the parameter, base temperature, T_{base} (which is temperature at 20 ka). n), o), and p) represent histograms of present temperature, $T_{present}$ (which is $T_{base}+T_{amp}$ as shown in supplement Eq. S9). These results are obtained using the kinetic parameters of sample MBTP9.

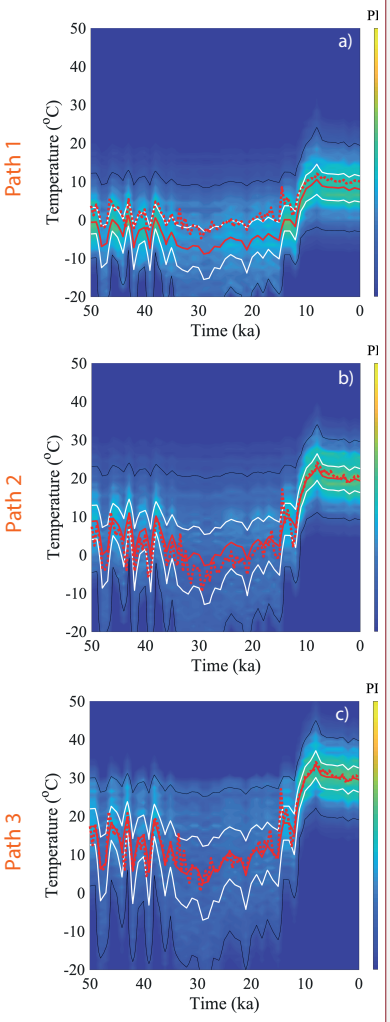

Figure 7: Result of synthetic experiments for the three thermal histories shown in Fig. 6. a), b) and c

Deleted: d), e
Deleted: f
Deleted:).
Deleted: ¶
Deleted: d), e
Deleted: f
Formatted

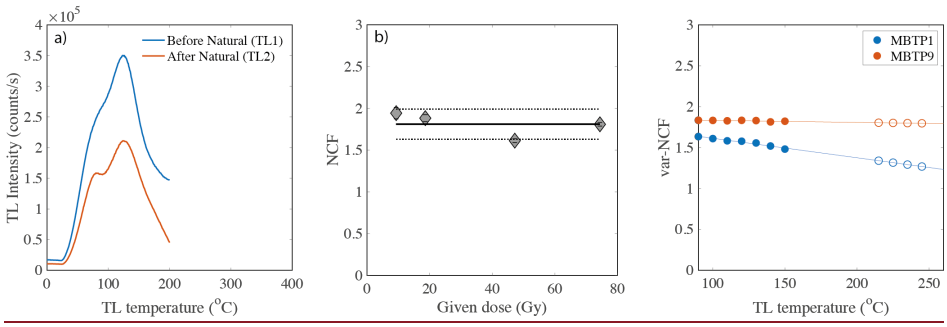

Figure 8: a) The lower temperature TL before (TL_1) and after (TL_2) natural TL measurement (up to 450 °C) of samples MBTP1 and MBTP9. b) NCF for TL signal (integrated over 90-120 °C) for different given doses. The data are scattered and vary within ±10%, which possibly suggest the NCF is dose independent c) plot of var-NCF (=TL_1/TL_2) at different temperature (90-150 °C) along TL glow (solid circles), and extrapolated to calculate NCF in the region of interest (210-250 °C; empty circles). The values were calculated by taking the average of three measurements.

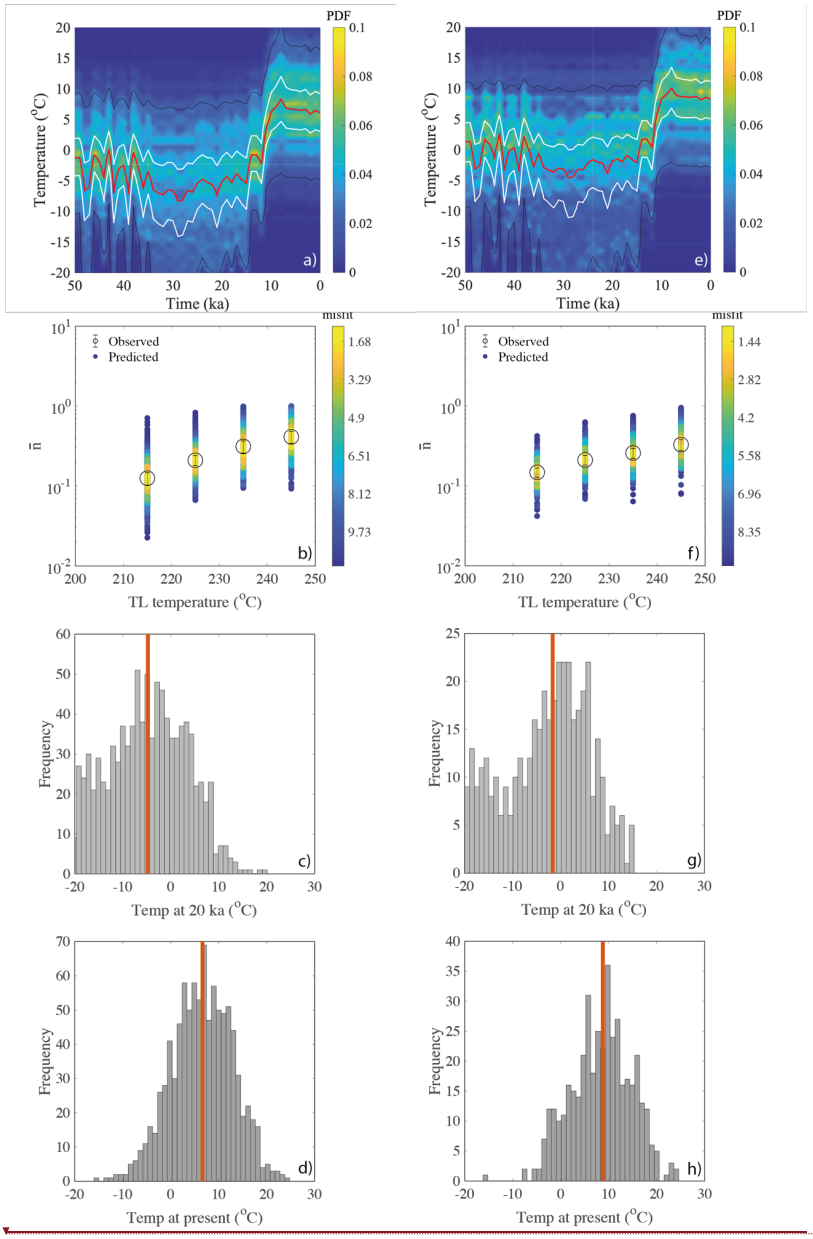

Deleted:

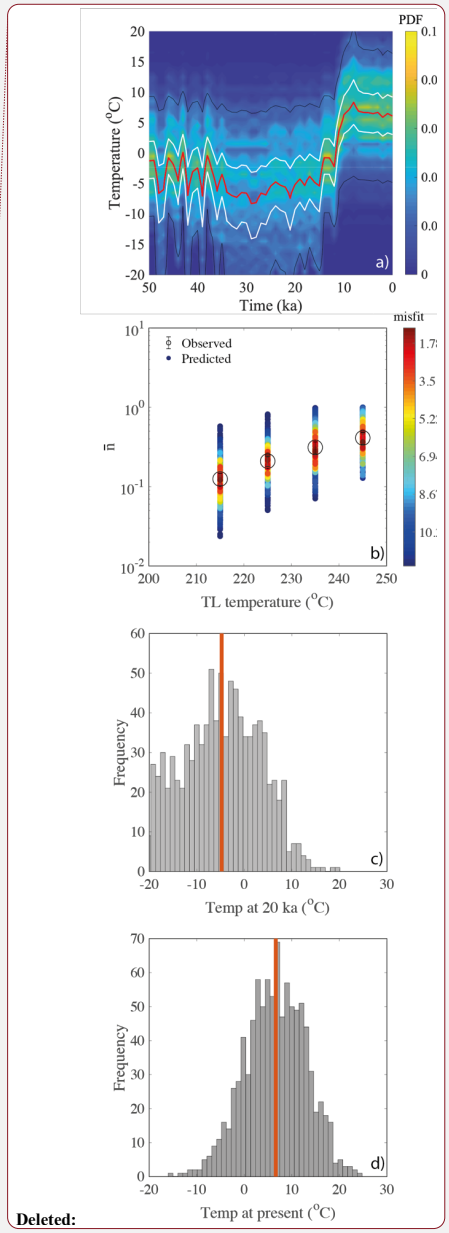

Figure 9: Inferred rock surface temperature history for sample MBTP1 and MBTP9 collected in the Mont Blanc massif at an altitude of ~2.0-2.5 km obtained through inverse modeling of TL data as described in section 4.4. a-d are for the sample MBTP1. a) is the probability density function. The red line, white lines and black lines are the predicted median, 1σ and 2σ confidence intervals. b) is the plot of observed TL ($\bar{n}_{obs}$) and modeled TL (predicted TL through inverse modeling). c) and d) are histograms of temperature at 20 ka and present respectively. e-h are the result of same analysis for sample MBTP9.

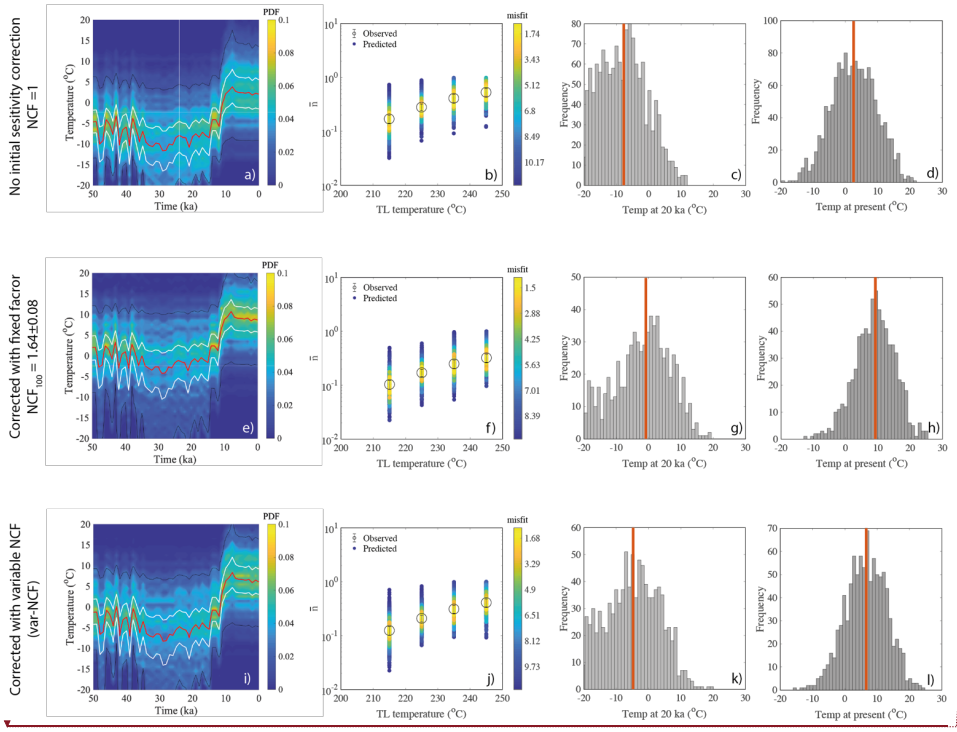

Deleted:

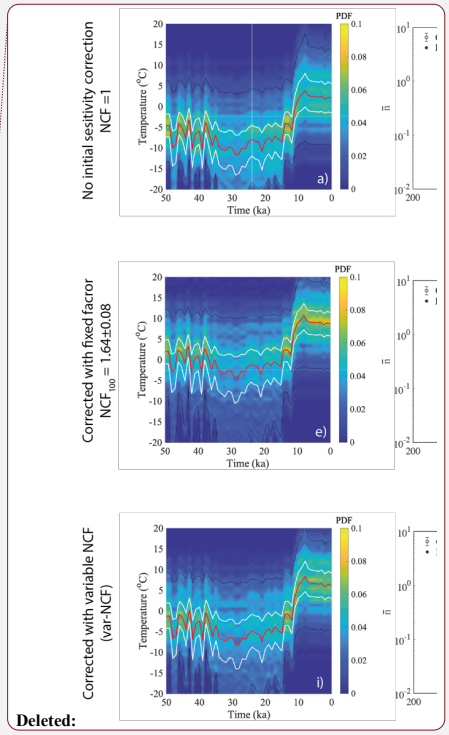

Figure 10: The impact of initial sensitivity correction for past temperature prediction to sample MBTP1 for three different scenarios, 1) no initial sensitivity correction i.e. NCF =1, 2) initial sensitivity corrected with fixed NCF at 100 °C (=1.64±0.08) for all thermometers, and, 3) initial sensitivity corrected to all TL thermometers with var-NCF for all TL thermometers (i.e. the selected method). a, e and i are the probability distributions, and b, f and j are observed and predicted TL plots for all three scenarios respectively. c, g, k and d, h, l are the histogram of predicted temperature for all accepted paths at 20 ka and the present day for all three scenarios respectively.

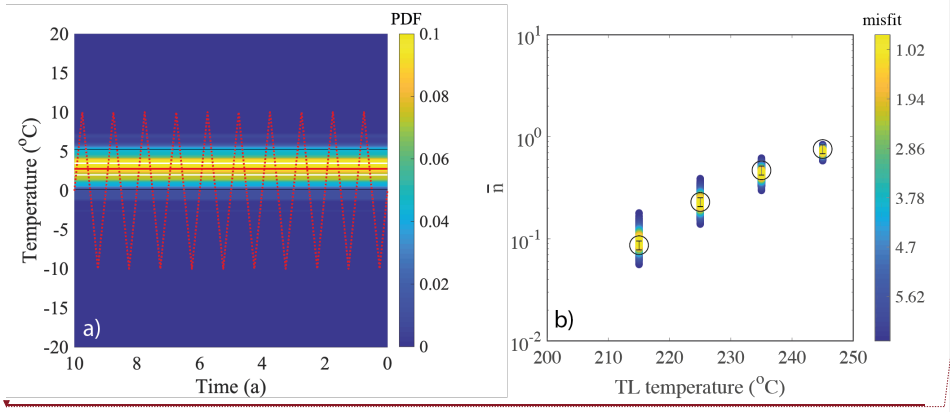

Deleted:

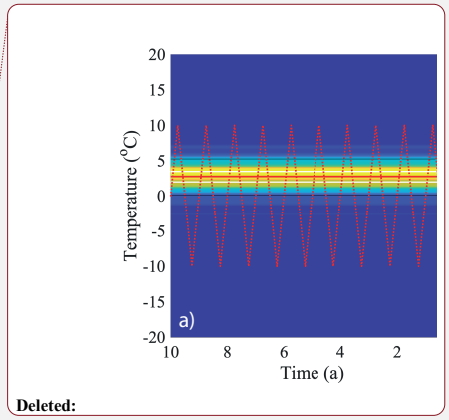

Figure 11: Result of synthetic test for annual fluctuation of temperature. a) probability density plot. The dotted redline is the actual thermal history. Solid red line is the predicted median of the isotherms. white and black lines are the 1σ and 2σ confidence intervals. Fig. b shows the plot of observed ($\bar{n}_{obs}$) and modeled TL values (predicted TL through inverse modeling) for all TL thermometers.

Table1: List of kinetic parameters that describe growth ($\dot{D}$, D_0, a), thermal decay (E, s, b) and athermal decay (ρ') and natural TL (observed) trapped charge populations ($\bar{n}_{obs}$) for the four thermometers (210-250 °C, 10 °C interval) for sample MBTP1 and MBTP9. The dose rate ($\dot{D}$) values were taken from Lehmann et al. (2020). Note that in the thermal decay parameters (*E*, *s* and *b*) no errors are mentioned. The mean values of these parameters are calculated from the distribution and an arbitrary error of 5% was considered.

		Growth			Thermal decay			Athermal decay	Natural TL ($\bar{n}_{obs}$)		
	TL (°C)	$\dot{D}$ (Gy/ka)	D_0 (Gy)	a	E (eV)	$\log_{10}(s)$	b	$\log_{10}(\rho')$	Uncorrected	NCF	Corrected
MBTP1	210-220	7.39 ± 0.16	766 ± 51	1.00 ± 0.09	1.24	11.62	1.46	-6.02 ± 0.08	0.17 ± 0.03	1.36 ± 0.04	0.13 ± 0.02
	220-230		690 ± 46	1.00 ± 0.11	1.28	11.69	1.45	-6.29 ± 0.14	0.28 ± 0.04	1.34 ± 0.03	0.21 ± 0.03
	230-240		638 ± 43	1.00 ± 0.13	1.31	11.75	1.45	-7.10 ± 0.94	0.41 ± 0.07	1.31 ± 0.03	0.31 ± 0.05
	240-250		559 ± 40	1.00 ± 0.26	1.35	11.79	1.45	<-20 ± 0	0.53 ± 0.09	1.29 ± 0.03	0.41 ± 0.07
MBTP9	210-220	7.07 ± 0.15	773 ± 41	1.00 ± 0.03	1.25	11.63	1.49	-6.13 ± 0.09	0.26 ± 0.03	1.73 ± 0.08	0.15 ± 0.02
	220-230		680 ± 37	1.00 ± 0.01	1.29	11.72	1.49	-6.18 ± 0.10	0.36 ± 0.05	1.72 ± 0.08	0.21 ± 0.03
	230-240		625 ± 40	1.18 ± 0.33	1.32	11.79	1.49	-6.33 ± 0.17	0.44 ± 0.06	1.71 ± 0.09	0.26 ± 0.04
	240-250		502 ± 36	1.10 ± 0.27	1.36	11.85	1.49	-6.51 ± 0.24	0.56 ± 0.08	1.70 ± 0.09	0.33 ± 0.05

Deleted: 2019b